Eng. Sci., 2025, **34**, 1442

Engineered Science
DOI: https://dx.doi.org/10.30919/es1442

Structural–Kinetic Analysis of Local Wild-Type and Mutants of Thermophile GH43 Bifunctional β-D-Xylosidase/α-L-Arabinofuranosidase

Rahmat Eko Sanjaya,[1, 2, 4] Ika Fitriani Juli Palupi,[3, 5] Ali Rohman,[2, 3] Lanny Hartanti,[2, 6] Rosli Md. Illias,[7, 8] Kazuhito Fujiyama[9] and Ni Nyoman Tri Puspaningsih[2, 3,*]

Abstract

Xylan is a renewable component of hemicellulose, consisting of xylose linked by β–1,4 glycosidic bonds. Complete xylan degradation requires various xylanolytic enzymes, including β–xylosidase. GbtXyl43A, GH43 thermophilic bifunctional β-xylosidase/α-L-arabinofuranosidase derived from Geobacillus thermoleovorans IT-08, uses Glu-177 and Asp-14 as catalytic residues, with Asp-121 playing a pivotal role in catalysis. Mutations in Asp-121 reduced its stability and activity. Asp-121 mutation to glutamic acid (D121E), asparagine (D121N), or valine (D121V) diminished the structural stability of GbtXyl43A. The 3D structure of GbtXyl43A and its mutants at pH 6.0 showed a predominantly negative charge at Asp-121, indicating altered electrostatic charge distribution near the active site, affecting its catalytic function. Molecular docking simulations of GbtXyl43A and D121N, yielding binding energies of −7.2 kcal/mol and −6.7 kcal/mol. The kinetic parameters of GbtXyl43A and D121N were V_{max} (3.35 × 10^{-3} and 0.10 × 10^{-3} mM/min), K_M (2.84 and 4.56 mM), k_{cat} (1.97 and 8.40 × 10^{-4} min^{-1}), and kcat/KM (0.69 and 1.84 × 10^{-4} $min^{-1}mM^{-1}$). In-silico approach and analogous residue analysis indicated that Asp-121 functions as a pKa modulator essential for GbtXyl43A stability and catalytic activity. This study enhances the understanding of Asp-121 as the secondary aspartic acid residue that forms the catalytic triad of GH43 β-xylosidase.

Keywords: Renewable component; GH43 thermophilic bifunctional β-Xylosidase/α-L-arabinofuranosidase; Geobacillus thermoleovorans IT-08; GbtXyl43A; Wild type-mutant; Kinetic characterization.

Received: 12 January 2025; Revised: 17 February 2025; Accepted: 27 February 2025.
Article type: Research article.

1. Introduction

Lignocellulose is a heterogenous polymer composed primarily of lignin, cellulose, and hemicellulose.[1] Lignocellulose is an underutilized waste product from agro-industrial processing. The carbohydrate content in the form of cellulose and hemicellulose reaches approximately 75 – 85%, making it a potential abundant as renewable energy resources for developing environmental sustainability.[2,3,4] Hemicellulose is the most extensive renewable component in lignocellulose. Hemicellulose is also favourable for energy-related applications and is recommended to isolate from biomass by enzyme-aided methods. Hemicellulose is divided into hardwood and softwood. Hardwood is composed of *O*-acetyl-4-*O*-methylglucuronoxylan, glucomannan, and xyloglucan. While softwood consists of *O*-acetyl-galactoglucomannan, arabinoglucuronoxylan, and arabinogalactan.[5] Xylan, is a complex polysaccharide, and a major component of hemicelluloses, consisting of xylose linked by β–1,4 glycosidic bonds that form its main chain.[6,7] The primary structure of xylan comprises β–xylopyranose residues modified by substituent groups such as acetyl, arabinosyl, and glucuronyl. Xylan might be hydrolyzed into a monomeric sugar by xylan-degrading enzymes, or xylanases, which are abundantly produced by bacteria and fungi.[8–13] Xylanases are

[1] *Mathematics and Natural Science Study Program, Faculty of Science and Technology, Universitas Airlangga, Surabaya, 60115, Indonesia*
[2] *Proteomic Laboratory, University-CoE-Research Center for Bio-Molecule Engineering, Universitas Airlangga, Surabaya, 60115, Indonesia*
[3] *Department of Chemistry, Faculty of Science and Technology, Universitas Airlangga, Surabaya, 60115, Indonesia*
[4] *Department of Chemistry, Faculty of Mathematics and Natural Science, Universitas Lambung Mangkurat, Banjarbaru, 70714, Indonesia*
[5] *Mineral Chemical Engineering, Metal Industry Polytechnic of Morowali, Morowali, 94974, Indonesia*

members of the glycoside hydrolase (GH) family. These enzymes catalyze β–1,4 glycosidic bond hydrolysis within xylosides, releasing hemiacetal and aglycones—non-sugar molecules generated when the glycosyl group in glycosides is replaced by hydrogen atoms.[14] Complete xylan hydrolysis requires various xylanases with specific catalytic roles. These enzymes include endo–β–xylanase (EC 3.2.1.8), β–xylosidase (EC 3.2.1.37), α–L–arabinofuranosidase (EC 3.2.1.55), acetyl xylan esterase (EC 3.1.1.72), feruloyl esterase (EC 3.1.1.73), and α-glucuronidase (EC 3.2.1.39),[15] which function synergistically to completely degrade xylan into its constituent monomers.

β–xylosidase is a xylan-degrading enzyme with exo-xylanase activity hydrolyzing 1,4–β–D–xylooligosaccharides to xylose from non-reducing end.[14,16] However, xylan could not be hydrolized directly by β–xylosidase. Xylobiose or xylooligosaccharides are frequently as the β-xylosidase substrate, and the affinity to the substrate is inversely proportional to the polymerization degree. The enzyme also hydrolyzes synthetic substrates such as *p*–nitrophenyl– and *o*–nitrophenyl–β–D–xylopyranoside. β–Xylosidase is classified into various GH families, including GH 1, 3, 5, 30, 39, 43, 51, 52, 54, 116, and 120.[14] GHs (EC 3.2.1.-) are well-characterized enzymes that hydrolyze glycosidic bonds between two or more carbohydrates or between carbohydrates and non-carbohydrate groups (http://www.cazy.org/Glycoside-Hydrolases.html). The grouping of enzymes into the GH family is based on the conserved of amino acid sequences.[17,18] Enzymes in the same family show have the similar amino acid sequence and three-dimensional (3D) structures.

GbtXyl43A is a thermophilic bifunctional β-xylosidase/α-L-arabinofuranosidase isolated from *Geobacillus thermoleovorans* IT-08 with optimum activity at pH 6.0 and 50 °C.[19,20] GbtXyl43A exhibits dual activities as both β–D–xylosidase and α–L–arabinofuranosidase. The enzyme belongs to member of the GH43 family, containing a catalytic residue Asp-14 and Glu-177 as the catalytic base and acid, respectively.[21] In addition, GH43 β–xylosidase exhibits third catalytic residue, which acts as a p*K*a modulator directing the β-xylosidase enzyme to the substrate.[22] In a previous study, GbtXyl43A was generated by substituting Asp-121, which functions as a p*K*a modulator, with asparagine (Asn), glutamic acid (Glu), and valine (Val), The decreased activity of the variant indicated that Asp-121 plays a central role in regulating catalytic GbtXyl43A activity.[23] Therefore, the variant potentially exhibits a lower affinity than the wild-type. In this study, the effects of mutation Asp-121on stability and kinetics of the enzymes were investigated by analyzing both variables using in silico and in vitro approaches to determine their kinetic parameters.

[6] *Department of Pharmacy, Faculty of Pharmacy Universitas Katolik Widya Mandala, Surabaya, 60112, Indonesia*
[7] *Institute of Bioproduct Development, Universiti Teknologi Malaysia, Skudai, 81310, Malaysia*
[8] *Faculty of Chemical and Energy Engineering, Universiti Teknologi Malaysia, Skudai, 81310, Malaysia*
[9] *International Center for Biotechnology (ICBiotech), Osaka University, Osaka, 565-0871, Japan*
**Email:* ni-nyoman-t-p@fst.unair.ac.id (N. N. T. Puspaningsih)

2. Materials and methods

2.1 Protein stability and the effect of mutation on residue energy

The I-Mutant v2.0,[24] MUpro,[25] SAAFEC-SEQ,[26] iStable,[27,28] DUET,[29] and CUPSAT,[30] web servers were used to predict the effect of amino acid changes on GbtXyl43A. I-Mutant v2.0 is a support vector machine-based web server used to automatically predict protein stability changes upon single-site mutations using protein sequences (https://folding.biofold.org/cgi-bin/i-mutant2.0.cgi). The MUpro server is used to predict protein stability changes in single-site mutations from sequences (https://mupro.proteomics.ics.uci.edu/). SAAFEC-SEQ is an online application used to calculate folding free-energy changes in proteins caused by mutations (http://compbio.clemson.edu/SAAFEC-SEQ/index.php#started). iStable is an integrated protein stability predictor that uses sequence information and prediction results from different element predictors (http://predictor.nchu.edu.tw/istable/indexSeq.php). In addition to the FASTA format, the PDB format is also available to predict protein stability. DUET (https://biosig.lab.uq.edu.au/duet/stability) and CUPSAT (https://cupsat.brenda-enzymes.org/index.jsp) are web servers used to predict protein stability caused by amino acid changes. DUET produces data in mCSM, SDM, and DUET. CUPSAT is used to predict changes in protein stability based on amino acid–atom potentials and torsion angle distributions to evaluate the amino acid environment of the mutation site.

The Asp-121 mutation in GbtXyl43A influences neighboring residues that may act as stabilizers or destabilizers, indicated by the relative energy produced at each site. The Mutation Explorer server (https://mutationexplorer.vda-group.de/mutation_explorer/submit) was used to determine the effects of mutations on the surrounding residues.[31] The Mutation Explorer server uses the PDB format as the output and determines the mutated amino acids. A negative residue

value indicates that the residue is a stabilizer, whereas a positive value indicates that it is a destabilizer. The resulting value is expressed as relative energy in Rosetta Energy Units (R.E.U).

2.2 Molecular modeling and stereochemical evaluation

GbtXyl43A is a native protein whose 3D structure is based on the Protein Data Bank (PDB ID 5Z5I) and was used as a template for modeling the variant structure. GbtXyl43A contains 510 amino acids. Substitutions were introduced at position 121, where Asp-121 was replaced with Asn (D121N), Glu (D121E), and Val (D121V). 3D structures of complete GbtXyl43A and mutants were generated using the SWISS-MODEL server (https://swissmodel.expasy.org/).[32–35] The GbtXyl43A and mutant structures were saved as PDB files, subjected to energy minimization using Gromos96 tools in Swiss-PdbViewerthen used for stereochemical evaluation, electrostatic surface potential analysis, and molecular docking.[36,37]

Protons were added or removed in the energy-minimized model to simulate the charge state of the model under various pH conditions (pH 6.0 and 9.0) using the H++ server (http://newbiophysics.cs.vt.edu/H++/uploadpdb.php).[38,39] The H++ server is an automated system that computes the p*K* values of ionizable groups in macromolecules and adds missing hydrogen atoms based on the specified pH of the environment. The protonation state of the model was determined based on the calculated ionizable side chain ionization states at a specified pH. The output from H++ was a PDB (PQR) structure in a predicted protonation state, with protonation states at pH 6.0 and 9.0, salinity 0.15, internal dielectric 10, and external dielectric 80.

The quality of the structural models was evaluated using the PROCHECK and ERRAT servers (https://saves.mbi.ucla.edu/).[40] PROCHECK was used to evaluate the stereochemical quality of the protein structures by analyzing the residue-by-residue and overall structural geometries; the results are presented as a Ramachandran plot. ERRAT values were used to assess the protein structure resolution. Values of ≥ 95% indicated high-resolution structures, whereas values approximating 91% indicated lower resolutions (2.5 to 3.0).[41] ProSA-web was used to assess the *Z* score and energy plots (https://prosa.services.came.sbg.ac.at/prosa.php).[42] The desirable *Z* score should be < 1 compared to the non-redundant set of PDB structures. QMEAN4 was used to calculate the cumulative QMEAN values on a global scale (range: 0–1).[43] Verify3D was used to determine the compatibility of an atomic model (3D) with its amino acid sequence (1D) by assigning a structural class based on its location and environment and comparing the results to good structures. The models were visualized using PyMOL (PyMOL Molecular Graphics System, Version 2.5.8; Schrödinger, LLC).

2.3 Electrostatic surface potential analysis

The electrostatic surface potential of GbtXyl43A and its mutants was assessed under different pH conditions using the Adaptive Poisson–Boltzmann Solver (APBS) plugin in the PyMOL software (PyMOL Molecular Graphics System, Version 2.5.8; Schrödinger, LLC). The electrostatic surface potential of the protein was calculated by numerically solving the Poisson–Boltzmann equation using point charges based on molecular mechanics. Electrostatic potential maps of the protein under different pH conditions were generated using a coloring scheme that tinted the protein surface based on the overall charge distribution.

2.4 Molecular docking

The 3D structure of *p*–nitrophenyl β–D–xylopyranoside (*p*NP–X; PubChem CID: 91509) was obtained from the PubChem database (http://pubchem.ncbi.nlm.nih.gov/) and used for docking simulations. The molecule was obtained in Simple Data Format from PubChem in 3D conformation and converted into MOL files using MarvinSketch© v6.0.0 software (ChemAxon Ltd). The molecules were subjected to energy minimization using an MMFF94 force field. Docking simulations were performed using the AutoDock Vina software.[44,45] A simulation of GbtXyl43A and its mutants was prepared using AutoDock Tools v1.5.7 before docking simulations. The receptor preparation process involved the addition of polar hydrogen atoms and force-field charges. The prepared receptors and ligands were stored in the PDBQT format. The binding region was defined using the Autogrid tool in Autodock with a spacing of ± 0.994 Å, coordinates of dimension $X = 22$, $Y = 22$, $Z = 22$, and a center of $X = 20.337$, $Y = -40.839$, $Z = 17.826$. Docking analysis was performed using the Lamarckian Genetic Algorithm with 100 docking runs, and the best result was selected as the lowest binding energy. The protein–ligand complexes and their molecular interactions were visualized using PyMOL (PyMOL Molecular Graphics System, version 2.5.8; Schrödinger, LLC), and two-dimensional visualization was performed using LigPlot+© v2.2.8.[46]

2.5 Purification and kinetic properties

Escherichia coli BL21 containing the *GbtXyl43a* and *D121N* genes belongs to Proteomic Laboratory, University CoE-Research Center for Bio-Molecule Engineering, Universitas

Airlangga, Surabaya, East Java, Indonesia. *Escherichia coli* BL21 harboring the genes encoding GbtXyl43A and D121N were inoculated into Luria–Bertani medium containing ampicillin. Cultures were incubated at 37°C with shaking at 150 rpm. Isopropyl β–D–1–thiogalactopyranoside (1 M) was added when the OD_{600} reached 0.5–0.8. The culture was then re-incubated at 37 °C for 3 h for GbtXyl43A and 6 h for D121N. The GbtXyl43A and D121N proteins were isolated by lysis and centrifuged at 4 °C to obtain supernatants containing the GbtXyl43A and D121N proteins.

GbtXyl43A- and D121N-containing supernatants were purified using affinity chromatography on a Ni-NTA agarose column. The Ni-NTA column was washed and equilibrated using ultrapure water and phosphate buffer (pH 8.0 [50 mM phosphate buffer pH 8.0, 250 mM NaCl, and 10 m*M* imidazole]). After washing and equilibrating, GbtXyl43-containing supernatant was loaded onto a Ni-NTA column and incubated at 4 °C for 1 h to allow protein binding. The flow-through was collected every 1 h. The resin was eluted using an elution buffer with increasing imidazole concentrations. D121N purification was continued by anion-exchange chromatography (Toyopearl® DEAE-650M, Merck). Pre-equilibration was performed using Tris-buffer, pH 8.0. The D121N fraction was applied onto an anion-exchange column and eluted using a linear gradient of 0-0.5 M NaCl concentrations in Tris-buffer. The results of the elution with GbtXyl43A and D121N were analyzed using sodium dodecyl-polyacrylamide gel electrophoresis (SDS-PAGE).[47,48] The protein concentration was determined using the Bradford method.[49–52]

The enzyme kinetic parameters (K_M, V_{max}, k_{cat}, and k_{cat}/K_M) were measured by observing the absorbance changes of *p*NP–X at 405 nm. The hydrolysis reaction was determined by incubating the enzyme with *p*NP–X substrate at various concentrations (0.5–10 mM) at pH 6.0. The reaction was initiated by adding an enzyme solution to each substrate, which was then incubated at 50 °C. Each reaction was observed for 0–54 min. The initial velocity (V_0) of each substrate concentration was obtained from the linearity of each curve by plotting the incubation time vs. product concentration. Next, K_M, V_{max}, k_{cat}, and k_{cat}/K_M were determined using the Lineweaver–Burk plot.

3. Results and discussion

3.1 Point mutation on GbtXyl43A structure

GbtXyl43A belongs to a group of xylanolytic enzymes from the GH43 family with known 3D structures. GbtXyl43A is a *G. thermoleovorans* IT-08-derived β-D-xylosidase enzyme. Its overall fold is that of a five-bladed β-propeller, with Asp-14 functioning as the catalytic base and Glu-177 as the catalytic acid.[21,53] In contrast, Asp-121 is analogous to Asp-128 on XynB337,[22] which modulates the p*K*a of the catalytic acid to maintain it in the correct orientation. The Asp-121 residue in GbtXyl43A plays a pivotal role in modulating p*K*a and is essential for substrate binding and stabilization. A mutation was identified that determined the role of Asp-121 as a p*K*a modulator. The Asp-121 mutation disrupted the GbtXyl43A catalytic process, indicating the central role of Asp-121 and confirming it as Asp II or a third catalytic residue.

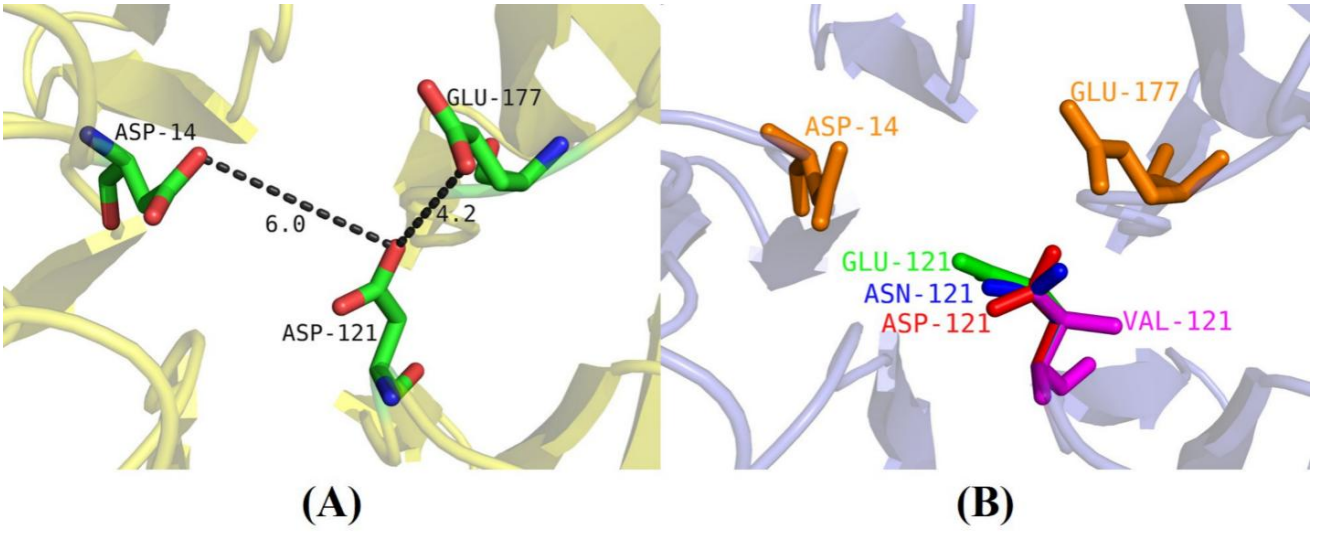

Fig. 1: GbtXyl43A, catalytic residue. (A) The distance between residues involved in the catalytic activities, with Asp-14 as the catalytic base, Glu-177 as the catalytic acid, and Asp-121, which modulates the p*K*a of the catalytic acid and maintains its correct orientation, (B) A comparison of residues in GbtXyl43A and the mutants. Asp-121 is a residue in GbtXyl43A (red), Glu-121 is a residue in D121E (green), Asn-121 is a residue in D121N (blue), and Val-121 is a residue in D121E (magenta). Asp14 and Glu177 are catalytic residues that act as nucleophiles and general acids/bases, respectively (orange).

The role of Asp-121 as the third catalytic residue was revealed by mutating Asp-121 into other residues, such as Glu, Asn, and Val, which represent amino acids with distinct chemical properties. They are negatively charged, polar uncharged, and hydrophobic, respectively. The mutants were identified as D121E (Asp to Glu), D121N (Asp to Asn), and D121V (Asp to Val) (Fig. 1). The effect of amino acid changes on the overall stability of GbtXyl43A was evaluated using mutant analysis. Stability is a crucial parameter to ascertain as it provides insights into the energy changes that occur in the GbtXyl43A structure owing to mutations. Energy variables are crucial in the context of protein stability and warrant particular attention.

Asp-121, as a p*K*a modulator, plays a crucial role in maintaining the correct orientation of the substrate on the catalytic side. Measuring the distance between each catalytic residue with Asp-121 showed that residue Asp-14 had a distance of 6.0 Å and Glu-177 had a distance of 4.2 Å (Fig. 1). The relatively close distance between Asp-121 and Glu-177, which acts as a general acidic residue, resulted in Asp-121 affecting Glu-177. In contrast, Asp-14 did not exert a marked effect, indicating that the p*K*a modulator Asp-121 affects the catalytic activity of the acidic residue Glu-177.

β-Xylosidase hydrolyzes the substrate using a mechanism that inverts the structure by the anomeric configuration. The catalytic active site of GbtXyl43A is located at one end of the funnel-shaped cavity of the β-propeller domain that is formed because of the β-sheet packing. Like other GH43 members, three acidic residues are essential for the catalytic activity of GbtXyl43A: Asp-14, the general base; Glu-177, the general acid; and Asp-121, which modulates the p*K*a and maintains the correct orientation of the general acid residue.[22,23] Unlike the classic paradigm of two essential catalytic residues in most GHs, five-bladed β-propeller GHs use an additional acidic catalytic residue that modulates p*K*a and orients the general acid catalytic residue.[54] Asp-121 is 4.2 Å from Glu177, enabling it to modulate the p*K*a of this residue,[55] keeping it protonated and allowing it to function as an acid for the reaction. Asp-14, located 6.0 Å from Asp-121, is less affected by Asp-121.

A single-residue mutation in GbtXyl43A caused a change in free energy, which altered the stability of the protein. D121E, D121N, and D121V were subjected to protein stability analyses to investigate the effect of point mutations on free energy changes. The I-Mutant v2.0, MUpro, SAAFEC-SEQ, iStable, DUET, and CUPSAT tools were used to determine protein stability (Table 1). The mutants exerted a destabilizing effect on the protein, indicated by reduced stability and an overall decrease in energy. As indicated by the I-Mutant v2.0, MUpro, SAAFEC-SEQ, and iStable tools, a more negative ΔΔG value ($\Delta\Delta G < 0$) indicated a greater destabilizing effect of the mutation. Conversely, the iStable tool indicated that a more positive ΔΔG value ($\Delta\Delta G > 0$) is associated with decreased stability. However, the D121V mutant displayed an increased value when assessed using the iStable tool. Nevertheless, this did not have a significant effect, as most prediction tools indicated a decreased or destabilizing effect in the presence of all mutants.

The prediction tools use the FASTA format as input. In addition to the FASTA format, some servers require the input of a PDB structure or ID. DUET and CUPSAT use the 3D structure of the mutants (Table 2). These results demonstrate variability in the stability of the mutant structure. Analysis of D121E indicated that all tools provided data indicative of a destabilizing effect, whereas the D121V mutant only exhibited destabilizing values in the results provided by CUPSAT. For the D121N mutant, the four servers exhibited two destabilizing and two stabilizing effects. However, the data in

Table 1: Stability predictions of GbtXyl43A mutants using various prediction tools and FASTA format as input.

Mutants	I-Mutant v2.0 (ΔΔG, kcal/mol)	MUpro (ΔΔG, kcal/mol)	SAAFEC-SEQ (ΔΔG, kcal/mol)	iStable (ΔΔG, kcal/mol)
D121E	–1.27 (Decrease)	–0.120 (Decrease)	–1.37 (Destabilizing)	0.640 (Decrease)
D121N	–2.70 (Decrease)	–0.484 (Decrease)	–1.14 (Destabilizing)	0.643 (Decrease)
D121V	–2.62 (Decrease)	–0.015 (Decrease)	–1.09 (Destabilizing)	0.668 (Increase)

Table 2: Stability score prediction of GbtXyl43A variants using PDB format as input.

Variants	mCSM (ΔΔG, kcal/mol)	SDM (ΔΔG, kcal/mol)	DUET (ΔΔG, kcal/mol)	CUPSAT (ΔΔG, kcal/mol)
D121E	–0.298 (Destabilizing)	–0.490 (Destabilizing)	–0.087 (Destabilizing)	–3.03 (Destabilizing)
D121N	–0.177 (Destabilizing)	0.24 (Stabilizing)	0.098 (Stabilizing)	–4.31 (Destabilizing)
D121V	1.097 (Stabilizing)	1.1 (Stabilizing)	1.485 (Stabilizing)	–4.8 (Destabilizing)

Table 2 indicate that the mutation had a destabilizing effect on the GbtXyl43A structure, confirming the central role of Asp-121 in modulating p*K*a and maintaining structural stability.

Protein instability caused by mutations is defined as the overall value of the residues that comprise the protein structure. Replacing the Asp-121 residue markedly affected the surrounding residues, particularly those near the mutation point. GbtXyl43A has an R.E.U value of 0.00 and is negative for some residues (Table 3), indicating that the residues in GbtXyl43A were in an optimal state. Introducing mutations at Asp-121 resulted in notable alterations in the R.E.U values of numerous residues, with most exhibiting relatively positive values, suggesting that these residues contributed to destabilizing the overall structure. In Mutation Explorer, a negative energy value indicates that a particular residue has a stabilizing effect on the overall structure. Similarly, mutations that reduce energy are regarded as stabilizing mutations. The Glu-121, Asn-121, and Val-121 energies were 17.81, 4.73, and 38.57 R.E.U., respectively, suggesting that the residue that replaced Asp-121 was destabilizing and affected the other residues. The energy value of Asp-14 in D121E was 1.40 R.E.U., whereas the other variants were undetected, indicating that the Asp-121 to Asn and Val mutation did not affect Asp-14. The acid catalytic residue, Glu-177, exhibited energy values of –0.41 R.E.U. and –0.85 R.E.U. in D121E and D121V, respectively. Although these values suggest that the mutation affects the stability of the Glu-171 residue, they do not necessarily imply that the resulting mutant is of greater quality than GbtXyl43A because the overall residue remained in a high-energy state.

This study aimed to confirm whether Asp-121, along with Asp-14 and Glu-177, forms a catalytic triad. In silico analysis began with structural stability assessments, as Asp mutations in the GH43 family affect enzyme activity. For example, Mutations in Asp-121[22] in β-xylosidase from *Geobacillus stearothermophilus* (XynB3), and in Asp-158M,[56] in arabinose from *Cellvibrio japonicus* (Arb43A) caused conformational changes, with Glu-187 in XynB3 and Glu-221 in Arb43A exhibiting altered rotations due to repulsive interactions. This rotation is exclusive to general acids, whereas the general base angle remains unaltered compared to its original conformation. These changes support the role of Asp in "guiding" the general acid into the correct orientation toward the substrate and modulating p*K*a.[22]

Computational analysis of the D121E, D121N, and D121V mutants using FASTA and PDB formats revealed destabilizing effects on the overall protein structure. Mutations that affect structural stability must exhibit a marked stabilizing or increasing value for each parameter or test program. Stability screenings indicated that Asp-121 mutations had destabilizing impacts, highlighting the essential role of Asp-121 in maintaining the structural integrity of GbtXyl43A and as a p*K*a modulator. Furthermore, the Asp-121 residue exhibited an energy value of 0.00 R.E.U. before the mutation. Notable energy fluctuations were observed when Asp-121 was replaced with Val, Glu, or Asn. The energy value with the greatest positive value indicated that these residues contributed to destabilization,[31] supporting the hypothesis that the mutation of Asp to Val, Glu, or Asn at position 121 results in structural instability.

Table 3: Changes in residue energy because of point mutations on the GbtXyl43A structure.

GbtXyl43A		D121E		D121N		D121V	
Residue	Energy (R.E.U)	Residue	Energy (R.E.U)	Residue	Energy (R.E.U)	Residue	Energy (R.E.U)
Asp14	0.00	Asp14	1.40	–	–	–	–
Pro15	–0.10	Pro15	0.26	–	–	–	–
Phe73	0.00	–	–	–	–	Phe73	0.13
Ala74	0.00	Ala74	10.58	Ala74	1.49	Ala74	–0.11
Pro75	–1.53	Pro75	–1.61	Pro75	–1.54	Pro75	–1.53
Ile120	0.00	Ile120	0.29	Ile120	–0.15	Ile120	11.74
Asp121*	0.00	Glu121*	17.81	Asn121*	4.73	Val121*	38.57
Pro122	–0.09	–	–	Pro122	–0.41	Pro122	4.61
Gly136	0.00	–	–	–	–	Gly136	–0.32
Thr137	0.00	–	–	–	–	Thr137	17.40
Glu152	0.00	–	–	Glu152	0.30	–	–
Leu166	0.00	–	–	–	–	Leu166	0.16
Glu177	0.00	Glu177	–0.41	Glu177	1.44	Glu177	–0.85
Ala178	0.00	Ala178	1.56	Ala178	2.75	Ala178	1.64
Pro179	–0.07	Pro179	–0.17	–	–	–	–
His180	0.00	His180	–0.20	–	–	–	–
His238	0.00	His238	7.32	His238	0.24	His238	0.16

*Native and mutant residues, R.E.U.; Rosetta Energy Units.

3.2 Modeling and stereochemical evaluation

Homology modeling was performed using the SWISS-MODEL to obtain a complete model of GbtXyl43A and its mutants. The wild-type structure was modeled because the initial crystallization structure contained fragments that were not modeled, specifically residues 305–310. Thus, homology modeling was used to obtain the complete structure. The structure of GbtXyl43A was previously determined using X-ray crystallography, and four protein structures were obtained, with one structure being the apo-enzyme (PDB ID 5Z5D) and three structures being complexes with ligands (PDB ID 5Z5F, 5Z5H, and 5Z5I).[21] The amino acid sequences of GbtXyl43A and its mutants (D121E, D121N, and D121V) were input into the SWISS-MODEL server, and the resulting tertiary structures were evaluated and assessed using computational tools. Figs. 2A and 3A show the 3D structures of GbtXyl43A and D121N, with red indicating α-helices and yellow indicating β-sheets. The β-sheet structure is the most abundant secondary structure in the GH43 family.

The quality of the tertiary structures of GbtXyl43A and its mutants was evaluated using QMEAN4, ERRAT, *Z* score, Ramachandran plot, and Verify 3D. Table 4 summarizes the quality parameters of the model structure after minimization using the Swiss-PdbViewer. A higher QMEAN4 score indicated a more stable structure, whereas a negative score indicated an unstable structure.[57] QMEAN4 predicts the global model structure quality based on a linear combination of four descriptors: local geometry, distance-dependent interaction, agreement between the predicted secondary structure and solvent accessibility, and solvation potential. The QMEAN4 values for GbtXyl43A and its mutants were 0.75–1.08, indicating that the structural model is of good quality.

Protein Structure Analysis (ProSA) is used to evaluate the accuracy of protein model structures for structural prediction. Statistical methods were used to examine the experimental protein structures by employing X-ray crystallography and nuclear magnetic resonance (NMR) spectroscopy. The validation result for the 3D structure is a *Z*-score. A 3D structure was considered to be accurate if it exhibited a *Z* score within the range of the experimental protein structure.[37] The resulting model *Z* score was from –8.75 to –8.68 (Table 4). The *Z* scores of GbtXyl43A and D121N were within the *Z* score range of the protein structure, as determined by X-ray spectroscopy (Figs. 2B and 3B). ERRAT and Ramachandran plots were used to assess the quality of the tertiary structure. The ERRAT values correlated with the resolution of the structures. High-resolution 3D structures typically yield values of ≥ 95%, whereas lower resolutions are observed when the average overall quality factor is approximately 91%. The overall quality factor of the model structure was > 91%,

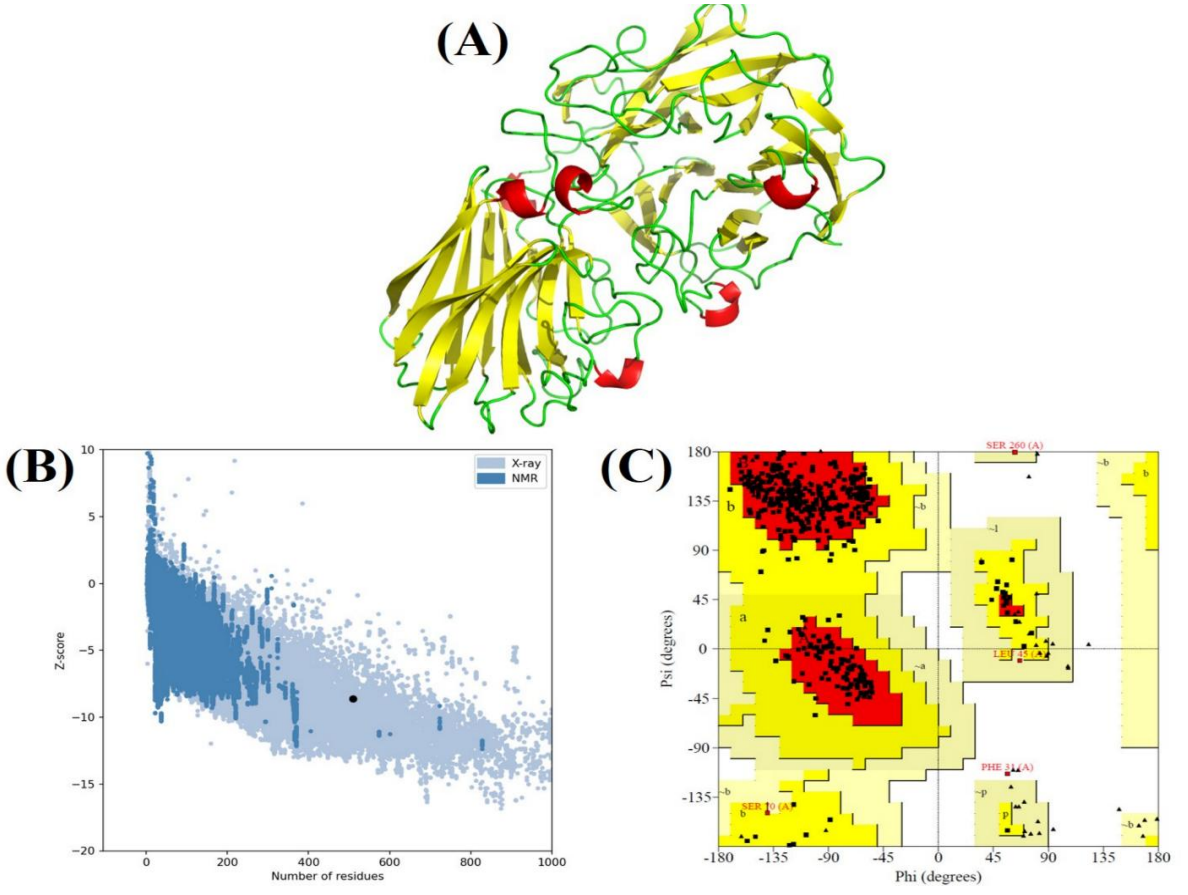

Fig. 2: Visualization of the structure and stereochemical properties of GbtXyl43A. (A) Structure of GbtXyl43A as modeled by SWISS-MODEL, (B) Ramachandran plot statistics showing the distribution of amino acids φ-ψ angles, (C) *Z* score value generated using the Protein Structure Analysis (ProSA) server.

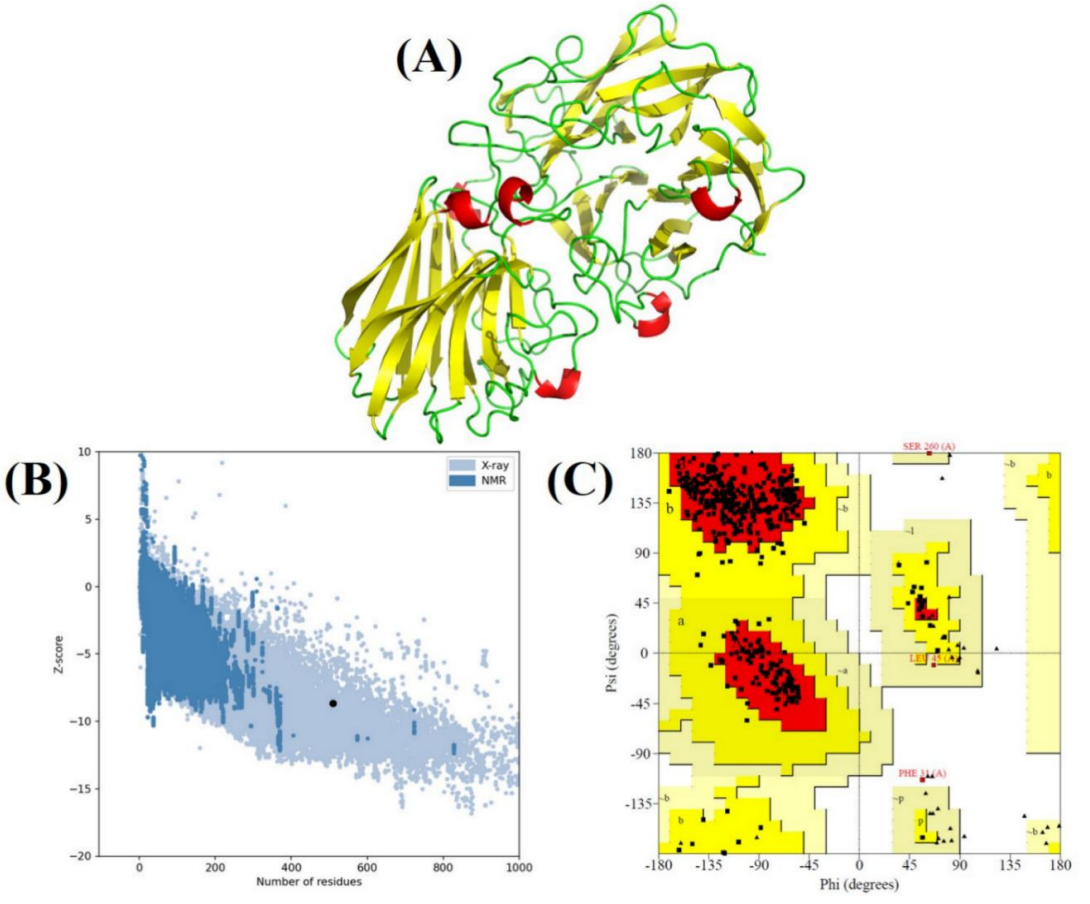

Fig. 3: Visualization of the structure and stereochemical properties of D121N. (A) Structure of D121N as modeled by SWISS-MODEL. (B) Ramachandran plot statistics showing the distribution of amino acids φ-ψ angles. (C) *Z* score value generated using the Protein Structure Analysis (ProSA) server.

indicating a relatively good structural resolution (Table 4). A model of good quality, as indicated by the Ramachandran plot, was expected to contain > 90% of the residues in the most favored regions. However, the residues in the favored regions of all models were < 90%. Figs. 2C and 3C illustrate the distribution of GbtXyl43A and D121N residues against φ and ψ angles in the Ramachandran plot.

The pH affects the cohesiveness of the protein structure. GbtXyl43A and mutant structures were assigned specific pH values using the H++ server, which computes the p*K* values of the ionizable groups in the macromolecules and adds absent hydrogen atoms according to the specified pH of the environment. The pH values used in this simulation were 6.0 and 9.0. pH 6.0 represents the optimal pH for GbtXyl43A, whereas pH 9.0 represents the optimal pH for D121N, which has lost approximately 18 times the activity specificity owing to the Asp to Asn mutation.[23] Several evaluation tools were implemented to assess the quality of the 3D structural models at pH 6.0 and 9.0. The Ramachandran plots generated by PROCHECK for all model structures at both pH 6.0 and pH 9.0 exhibited identical values but differed from those of the initial structure before pH adjustment (Tables 5 and 6).

Table 4: Comparison of QMEAN4, ERRAT, Ramachandran plot, and *Z* score for the quality assessment of three-dimensional structures after energy minimization using Swiss-PdbViewer.

Protein	QMEAN 4 score	ERRAT quality factor (%)	Ramachandran plot				*Z* score	Verify 3D (%)
			Residues in the most favored region (%)	Residues in additional allowed region (%)	Residues in generously allowed region (%)	Residues in disallowed region (%)		
GbtXyl43A	1.02	91.57	89.1	10.0	0.7	0.2	–8.70	89.61
D121E	0.94	91.77	89.3	10.0	0.5	0.2	–8.68	89.61
D121N	1.08	91.57	89.1	10.2	0.5	0.2	–8.75	89.61
D121V	0.75	91.37	88.8	10.2	0.7	0.2	–8.71	89.80

The pH affects the cohesiveness of the protein structure. GbtXyl43A and mutant structures were assigned specific pH values.

The φ-ψ values of 89.5% of the residues within the core region were in the most favorable region, whereas the φ-ψ values of 10.9% of the residues were within the allowed regions. Only 0.6% of the residues were in the generously allowed regions, whereas no φ-ψ values were observed for residues in the disallowed region. These findings suggest that the D121N model had good stereochemical quality at pH 6.0 and 9.0. This result is in contrast with the initial structure before incorporating the pH values, where only the φ-ψ values of 89.1% of the residues within the core region were in the most favorable region, and 0.2% of the residues were within the disallowed region. The φ-ψ values of the catalytic residues (Glu-177, Asp-14, and Asp-121) were in the fully allowed region, indicating that the model had good quality.

The overall ERRAT scores of the models at pH 6.0 and 9.0 exhibited comparable values of 92.37–93.37% for GbtXyl43A and the mutants (Tables 5 and 6). The score was higher than that of the original model before incorporating the pH values, indicating that the resulting models at pH 6.0 and 9.0 were within the range typically associated with high-quality models. Additionally, ERRAT analysis was valuable for analyzing protein structures, specifically regarding the number of non-bonded residues with a cutoff of 3.5 Å between different atom pairs. A high-resolution 3D structure was typically observed, with values of approximately 95% or higher. Lower resolution was observed when the average overall quality factor was approximately 91%. The ERRAT value of GbtXyl43A and mutant structures at pH 6.0 and 9.0 exceeded 92%, indicating that the structures generated at these pH values had relatively good structural resolution. An ERRAT value of < 91% indicates that the structure has a low resolution of approximately 2.5 to 3.0 Å. Therefore, a model structure with a value of > 92% has a resolution of < 2.5 Å. This value is sufficient for a protein structure in which the limit of acceptance of the crystallographic structures is a resolution of < 3.0 Å.

The quality of the model structure was evaluated using Verify 3D, which used a "3D-1D" profile based on the local environment of each lipase residue. The evaluation was based on statistical preferences regarding the buried area of each residue, the fraction of the side-chain area of each residue surrounded by oxygen, nitrogen, and other polar atoms (i.e., oxygen and nitrogen), and the local secondary structure assigned to each residue. Notably, the constructed model had satisfactory quality when the Verify 3D score was > 80%. All structures of GbtXyl43A and the mutants at pH 6.0 and 9.0 exhibited a Verify 3D score of > 80%, indicating that the overall quality of the side-chain environments was satisfactory. Structures of GbtXyl43A and its mutants at both pH values were of better quality than the model without pH adjustments. Given that pH 6.0 is the optimal pH for GbtXyl43A, molecular docking simulations can proceed with GbtXyl43A and D121N at this pH to explore ligand interactions. Kinetic analysis can also be performed to substantiate the hypothesis that Asp-121 functions as a catalytic triad and a p*K*a modulator.

3.3 Electrostatic surface potentials

Fig. 4 shows the electrostatic surface potentials of GbtXyl43A and its mutants at pH 6.0. A color scale represents the electrostatic surface potential; red indicates negatively charged regions, blue indicates positively charged regions, and white represents neutral areas. Arrows indicate the active sites involved in catalytic activity. Despite the diversity of their 3D folds, all structurally characterized β-xylosidase display a

Table 5: Comparison of the quality assessment parameters of three-dimensional structures at pH 6.0.

Protein	QMEAN 4 score	ERRAT quality factor (%)	Ramachandran plot				*Z* score	Verify 3D (%)
			Residues in the most favored region (%)	Residues in additional allowed region (%)	Residues in generously allowed region (%)	Residues in disallowed region (%)		
GbtXyl43A	1.16	93.37	89.5	9.7	0.8	0.0	–8.70	89.61
D121E	1.02	92.57	89.8	9.7	0.6	0.0	–8.68	89.61
D121N	1.33	92.37	89.5	10.0	0.6	0.0	–8.75	89.61
D121V	0.76	92.37	89.2	10.0	0.8	0.0	–8.71	89.80

Table 6: Comparison of the quality assessment parameters of three-dimensional structures at pH 9.0.

Protein	QMEAN 4 score	ERRAT quality factor (%)	Ramachandran plot				*Z* score	Verify 3D (%)
			Residues in the most favored region (%)	Residues in additional allowed region (%)	Residues in generously allowed region (%)	Residues in disallowed region (%)		
GbtXyl43A	1.16	92.37	89.5	9.7	0.8	0.0	–8.70	89.61
D121E	1.02	92.57	89.8	9.7	0.6	0.0	–8.68	89.61
D121N	1.33	92.37	89.5	10.0	0.6	0.0	–8.75	89.61
D121V	0.76	92.37	89.2	10.0	0.8	0.0	–8.71	89.80

typical pocket-shaped active site well-suited for exo-acting enzymes.[58] The pocket is negatively charged because of several acidic residues; however, it also contains hydrophobic patches of aromatic residues. This enzyme has a single route for the entry of substrates and the exit products.[14]

The 3D structures of GbtXyl43A and its mutants at pH 6.0 revealed the distribution of electrostatic charges around the active site, with a predominantly negatively charged region surrounding Asp-121. The mutation of Asp-121 resulted in alterations in the electrostatic charge distribution surrounding the active site, which affected the catalytic function of the enzyme. The charge distribution in GbtXyl43A revealed a markedly negatively charged area (red) near the active site, indicating the presence of Asp-121. This negative charge distribution plays a pivotal role in supporting the electrostatic interactions essential for the catalytic mechanism, particularly in stabilizing the protonation and deprotonation transitions of other catalytic residues, especially Glu-177. The disappearance of negative charges around the active site of D121E can affect the efficiency of the catalytic reaction. The p*K*a of Glu was slightly higher than that of Asp, which can cause Glu-121 in some protein states to be more protonated or more neutral than Asp-121 at the same pH, especially if local environmental influences modulate the p*K*a. Consequently, at pH 6.0, Glu-121 was more neutral than Asp-121, resulting in the reduction or even elimination of the negative charge previously present at that position. This causes the mutated region to appear blue, indicating that it is either neutral or slightly positively charged.

The mutation of Asp to Asn (D121N) results in the loss of the negative charge around the active site. The areas that should be negatively charged (red) change the charged state and become neutral (white). This alteration can disrupt interactions with substrates or other catalytic residues that rely on negative charges for optimal activity. Consequently, the catalytic activity may decrease markedly. The most substantial alteration in surface electrostatic charge distribution was observed in the D121V mutant. The overall reduction in the negative charge within the active site was striking, with a blue color (positive charge) being prevalent, indicating that the active site has lost much of the electrostatic interaction capacity necessary for catalysis, which may result in a substantial decline or even loss of enzyme activity.

In GH43 β-xylosidase, a secondary Asp residue acts as a p*K*a modulator often described as part of a catalytic triad.[59,60] The Asp residue plays a central role as a p*K*a modulator,

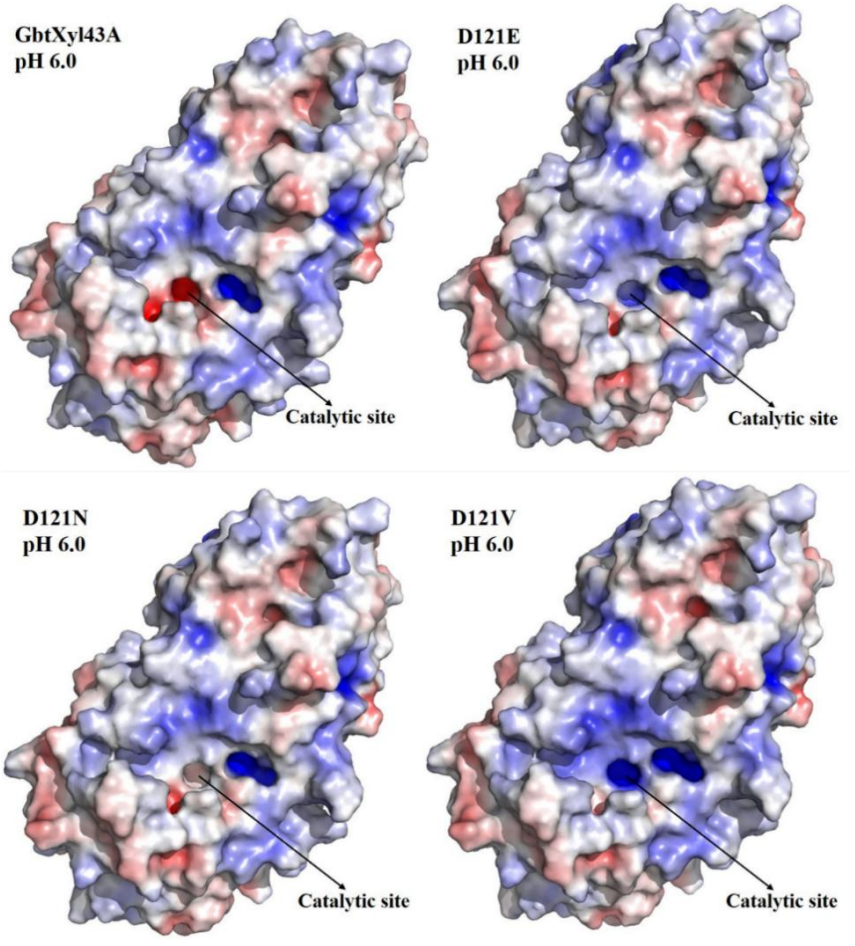

Fig. 4: Comparison of the electrostatic surface potential of GbtXyl43A and the mutants at pH 6.0. The range of electrostatic surface potentials is presented in a color gradient from red (negative potential) to blue (positive potential). The molecular surface is colored according to the electrostatic potential and computed using the Adaptive Poisson–Boltzmann Solver (APBS) within the PyMOL program. Red, blue, and white correspond to acidic (negative charge), basic (positive charge), and neutral potential, respectively.

facilitating equilibrium between protonation and deprotonation within the active site.[61] The electrostatic charge distribution on the surface of GbtXyl43A demonstrates the predominance of the negatively charged area surrounding Asp-121 (highlighted in red), which plays a pivotal role in maintaining the electrostatic environment essential for stabilizing the transition state and facilitating the Glu-177 protonation involved in the catalytic cycle.

In the inverse catalytic mechanism in the GH43 family, Glu-177 acts as a proton donor (catalytic acid) to release the glycosidic group from the ligand, whereas Asp-14 functions as a nucleophile that attacks the anomeric carbon of the ligand. This process forms a transition state that requires electrostatic stability, regulated by residues like Asp-121. Variations in the electrostatic charge distribution near Asp-121 could influence the inversion mechanism, affecting the ability of the catalytic residue to perform protonation and deprotonation effectively.

Although the amino acids are chemically similar, the substitution of Asp with Glu affects the electrostatic interactions and orientation near the active site, potentially affecting the catalytic role of Glu-177. This alteration in the inversion mechanism may not drastically reduce enzyme activity; however, it can decrease efficiency owing to altered electrostatic potential.[62,63] When Asp is replaced with Asn, the negative charge near the active site is lost because Asn is neutral, creating a markedly more neutral electrostatic environment,[64] potentially inhibiting the ability of Glu-177 to facilitate ligand protonation during the transition phase. The loss of negative charge from Asp-121 affects the stabilization of the nucleophilic residue Asp-14 and acidic residue Glu-177, substantially decreasing the catalytic activity because the crucial electrostatic interactions necessary for the transition were no longer available. Similarly, substituting the Asp residue with Val, a hydrophobic amino acid, resulted in a complete loss of negative charge at the active site. This result is indicated by the dominance of white and a slightly positive charge (blue), which alters the electrostatic environment of the active site. In the absence of sufficient electrostatic support, the nucleophile Asp-14 and acid Glu-177 were unable to function optimally, resulting in a drastic disruption of the catalytic mechanism.

Electrostatic charge distribution around active sites are crucial for successful catalysis. Stabilization of the transition state during glycosidic bond cleavage depends on electrostatic interactions controlled by residues near the active site, including Asp-121, a p*K*a modulator. Alterations in Asp-121, observed in D121E, D121N, and D121V mutations, directly affected charge distribution, impairing the catalytic efficiency of Glu-177 and Asp-14. Electrostatic potential calculations confirmed the crucial role of Asp-121 in catalysis, including its function as a p*K*a modulator and regulator of charge distribution in the active site. Mutations that change the charge properties of this residue result in substantial alterations in the electrostatic distribution, directly influencing the substrate-binding mechanism and catalytic reaction. This study demonstrates that Asp-121 mutation-induced electrostatic changes at pH 6.0 affect enzyme performance overall.

The electrostatic surface potential of the GbtXyl43A structure was examined at pH 9.0. Previously, the electrostatic charge distribution was examined at pH 6.0, the pH at which GbtXyl43A exhibits optimal activity.[23] The pH 9.0 value represents the optimum for the D121N and D121V mutants.[23] Thus, analyzing the electrostatic charge distribution of the two mutants was necessary. The response of each mutation to pH changes differed; consequently, the catalytic activity of the enzyme was affected. Fig. 5 illustrates the electrostatic surface potentials of D121N and D121V at pH 9.0. Compared to the active site area at pH 6.0, the active site area became more negative. The mutation of Asp to Asn (D121N), which results in the loss of the negative charge of Asp-121 and its replacement with a neutral Asn residue, caused a marked reduction in the negative electrostatic potential surrounding the active site. In such a situation, the charge distribution would be predominantly negative, originating from other residues such as Asp-14 and Glu-177. However, the mutant residue at position 121 did not contribute to this charge distribution. Replacing Asp with Val causes an imbalance in the charge distribution within the active site owing to the loss of the negative compensatory contribution of Asp, resulting in the redistribution of negative charges from other acidic residues such as Glu-177 and Asp-14. This redistribution can increase the local negative charge intensity of other acidic residues that remain deprotonated at pH 9.0. Many acidic residues, including Glu and Asp, were deprotonated at pH 9.0, indicating that these residues carried a full negative charge. In this context, the mutation of Asp to Val can facilitate redistribution, allowing acidic residues near the active site to increase their negative charge contribution, as indicated by the red markings.

At pH 9.0, altered charge distribution results in distinct responses for each mutant, influencing enzyme catalytic activity. Asn is neutral at physiological conditions and pH 9.0. However, aspartate is deprotonated and carries a negative charge. Asn did not change substantially at high pH; therefore, the D121N mutant produced a more neutral active site than GbtXyl43A at pH 9.0. The loss of the negative charge from Asp-121 and its substitution with neutral residues resulted in reduced negative electrostatic potential surrounding the active site. Under these circumstances, the distribution of charges is predominantly influenced by negative charges from other residues, such as Asp-14 and Glu-177, without a contribution from position 121. The absence of a negative charge at Asp-121 disrupts transition state stabilization and reduces the electrostatic support crucial for the optimal function of Glu-177 and Asp-14. At high pH, where protonation is already more challenging owing to the basic environment, the loss of a negative charge from Asp-121 further impairs the ability of Glu-177 as a proton donor, reducing the reaction efficiency. Thus, the D121N mutant demonstrated a more pronounced decline in catalytic activity at pH 9.0 than at pH 6.0, reflecting

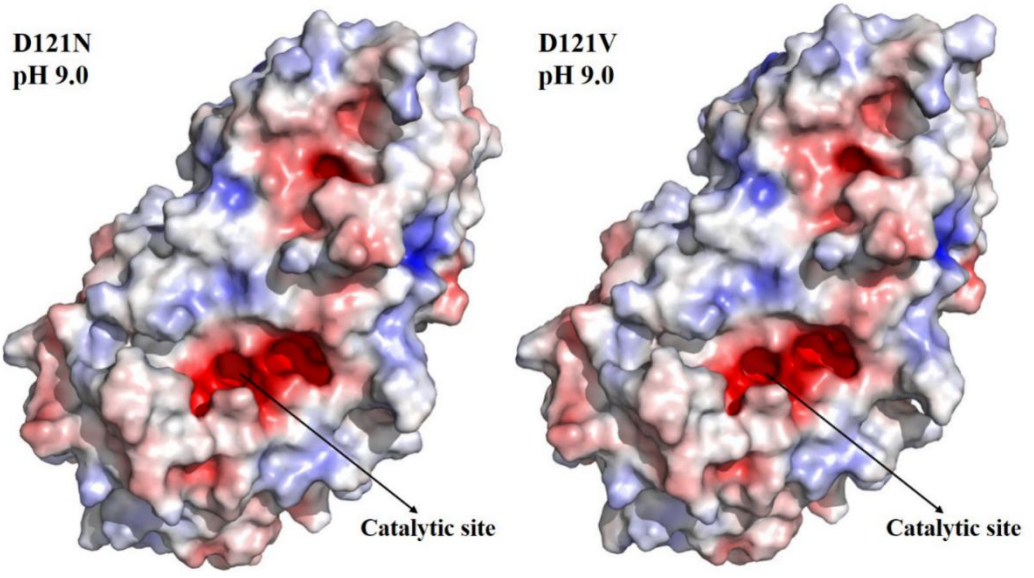

Fig. 5: Electrostatic surface potentials of D121N and D121V at pH 9.0. The range of electrostatic surface potentials is presented in a color gradient from red (negative potential) to blue (positive potential). The molecular surface is colored according to the electrostatic potential and computed using the APBS within the PyMOL program. Red, blue, and white correspond to acidic (negative charge), basic (positive charge), and neutral potential, respectively.

the amplified disturbance in protonation balance within the active site.

Val, a hydrophobic residue, remained uncharged across all tested pH values. The Val mutation completely negated the negative charge from Asp-121, affecting the efficiency of proton transfer and stabilization of the transition in the catalytic mechanism.[65,66] At pH 9.0, when most acidic residues (such as aspartate and glutamate) are deprotonated and negatively charged, the Val residue remains neutral and hydrophobic, resulting in neutral and hydrophobic active sites. The lack of the negative charge of Asp-121 exacerbates electrostatic imbalance within the active site, especially under basic conditions at pH 9.0, where the electrostatic contribution from Asp-121 becomes essential.

3.4 Molecular docking of GbtXyl43A and D121N

Molecular docking was used to determine the interactions between the active or binding side residues and ligands. The GbtXyl43A and D121N structure, at pH 6.0, were subjected to molecular docking with *p*NP–X using AutoDock Vina. The ten most favorable conformations for interaction with the enzyme-binding residue with the most negative affinity energy were identified for each ligand. The ligand conformation or pose with the most negative affinity energy was identified as the most favorable.

The binding analysis of GbtXyl43A and D121N to the *p*NP–X ligand revealed binding energies of –7.2 kcal/mol and –6.7 kcal/mol, respectively (Table 7), suggesting that the *p*NP–X ligand exhibited a higher affinity for GbtXyl43A than for D121N. This finding aligns with the results of the enzyme activity test, which showed that GbtXyl43A has a relatively high specific activity towards *p*NP–X compared with D121N.[23] These two findings, derived from the laboratory and in silico tests, reinforce the conclusion that Asp-121 plays an essential role in the catalytic function of GbtXyl43A. Five GbtXyl43A residues are involved in hydrogen bond formation with *p*NP–X, whereas D121N involves only four. In addition to hydrogen bonding, the interaction between GbtXyl43A, D121N, and the ligand also results in hydrophobic interactions. Seven residues were involved in hydrophobic interactions between the ligand and GbtXyl43A, whereas eight residues were involved in this process with D121N.

Notably, the formation of hydrogen bonds between GbtXyl43A and the ligand exhibited a distinct pattern, in which the triad of catalytic residues—Asp-14, Glu-177, and Asp-121—formed hydrogen bonds. In contrast, the D121N mutant only involved Asp-14 and Asn-121 in this process. This interaction provides insight into the functional equivalence of the wild-type and mutant residues in forming hydrogen bonds with the ligand. The distance between the two residues and the ligand did not differ substantially. The distance from Asp-121 to the O7 atom was 2.66 Å on the xylose ring, whereas that of Asn-121 was 2.73 Å (Fig. 6). Hydrogen bond formation on the same atoms was similar. The wild-type and mutant formed identical hydrogen bonds with the ligand through the same atom, indicating that the D121N mutant can maintain substrate binding similar to that of the wild-type regarding hydrogen interactions. However, the electrostatic and catalytic roles of Asp-121 as a p*K*a modulator cannot be entirely replaced by Asn-121 because Asn is a neutral residue and not negatively charged like Asp. Consequently, although the substrate may bind effectively, the catalytic efficiency of the enzyme will likely decline because of the loss of the capacity of Asp to facilitate protonation/deprotonation in the catalytic mechanism.

Molecular docking simulations of GbtXyl43A and D121N

at pH 6.0 with ligands revealed that the affinity of GbtXyl43A for the substrate was greater than that for D121N (Table 7). Notably, the Asp residue of GbtXyl43A and the Asn residue of D121N at position 121 both formed hydrogen bonds with the same atom of the ligand. Hydrogen bonds to the O7 atom are formed between Asp-121 and Asn-121 and the ligand at distances of 2.66 Å and 2.73 Å, respectively (Fig. 6). This result implies that ligand interactions are conserved in terms of bond geometry and molecular orientation and that Asn can maintain similar interactions with the ligand. Asn possesses a polar amide group (–$CONH_2$), enabling it to form hydrogen bonds despite its distinct chemical characteristics compared to the carboxylate group (–COOH) of Asp. The carboxylate group of Asp interacted with the ligand via a negatively charged moiety, whereas the amide group of Asn was neutral. Nevertheless, both the residues formed hydrogen bonds with the O atom of the ligand, indicating that despite the alteration in the chemical characteristics from negative to neutral charge, the capacity to form hydrogen bonds remained intact. The next implication is the stability of the enzyme–ligand complex. If both Asp-121 and Asn-121 form hydrogen bonds with the O7 atom of *p*NP–X, the stability of the enzyme-substrate complex in the D121N mutant likely does not change markedly compared to that in the wild-type. Although Asn-121 can form

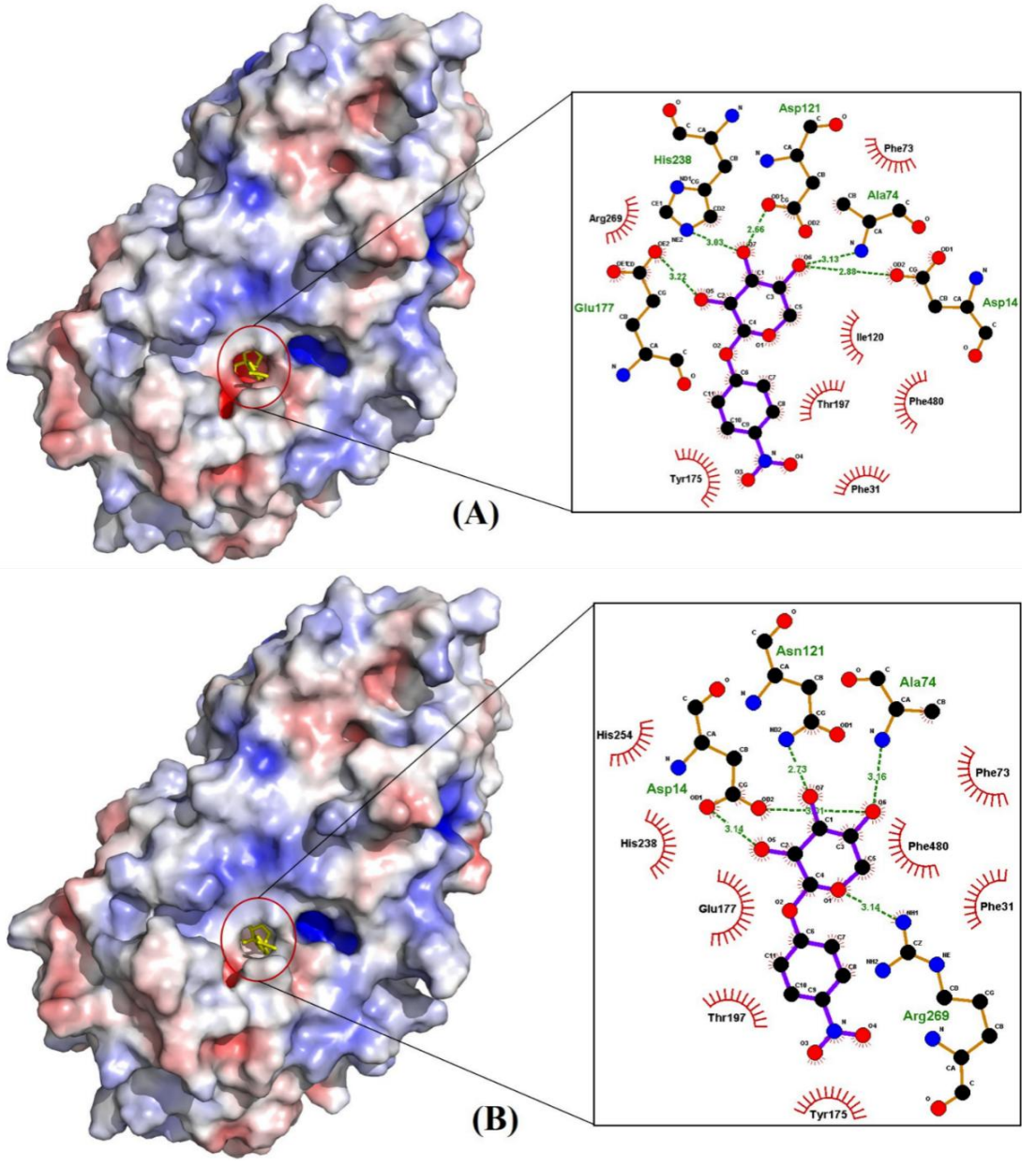

Fig. 6: Schematic representation of protein–ligand docked complexes. (A) GbtXyl43A–*p*NP–X docked complex (left) and the interacted amino acid residues (right), (B) D121N–*p*NP–X docked complex (left) and the interacted amino acid residues (right). The *p*–nitrophenyl β–D–xylopyranoside (*p*NP–X) ligand is represented by purple bonds. Dashed lines represent the hydrogen bond interactions, and their distances are indicated in Å. The amino acid residues involved in the hydrophobic interactions are shown as starbursts. Interaction analysis and figure preparation were performed using LigPlot+.

Table 7: Molecular docking analysis of GbtXyl43A and D121N with *p*–nitrophenyl β–D–xylopyranoside using Autodock Vina.

Protein	Affinity, (kcal/mol)	Hydrogen bonding		Hydrophobic interactions
		Residue	Distance (Å)	
GbtXyl43A	–7.2	Asp14	2.88	Phe31, Phe73, Ile120, Tyr175, Thr197, Arg269, Phe480
		Ala74	3.13	
		Asp121	2.66	
		Glu177	3.22	
		His238	3.03	
D121N	–6.7	Asp14	3.01, 3.14	Phe31, Phe73, Glu177, Tyr175, Thr197, His238, His254, Phe480
		Ala74	3.16	
		Asn121	2.73	
		Arg269	3.14	

hydrogen bonds, the transition from a negatively charged group (Asp) to a neutral group (Asn) may influence overall electrostatic interactions in the area surrounding the active site.

Asp-121 in GbtXyl43A has dual functions: hydrogen bond formation and electrostatic charge regulation within the active site, acting as a p*K*a modulator, which facilitates protonation/deprotonation during the catalytic cycle.[59] Despite retaining its capacity to form hydrogen bonds with ligands, Asn-121 lacks the electrostatic capability to act as a p*K*a modulator because of the absence of a negative charge. Consequently, despite the maintenance of comparable hydrogen bonds by Asn-121, the catalytic activity of the D121N mutant is likely diminished because of alterations in the protonation equilibrium and electrostatic stabilization within the active site. Therefore, although substrate-binding remains effective, the altered role of Asp-121 as a charge regulator may impair catalytic efficiency.

3.5 Purification and kinetic properties of GbtXyl43A and D121N

GbtXyl43A was purified using Ni-NTA affinity chromatography. Affinity chromatography comprises three principal stages: protein binding to resin, washing, and elution. The binding buffer contained a low imidazole concentration. The protein was released from the resin as the imidazole concentration increased. The results of GbtXyl43A purification are indicated by a single band on SDS-PAGE (Fig. 7) with an estimated molecular weight of ~58 kDa. GbtXyl43A exhibited a purity level that is 5 times higher than that of the cell-free extract. Purification of the D121N variant was performed using Ni-NTA affinity chromatography and ion-exchange chromatography. Ion exchange chromatography was performed because of the inability to obtain pure D121N using affinity chromatography. D121N purification results are shown by SDS-PAGE, which indicated a size of ~58 kDa (Fig.

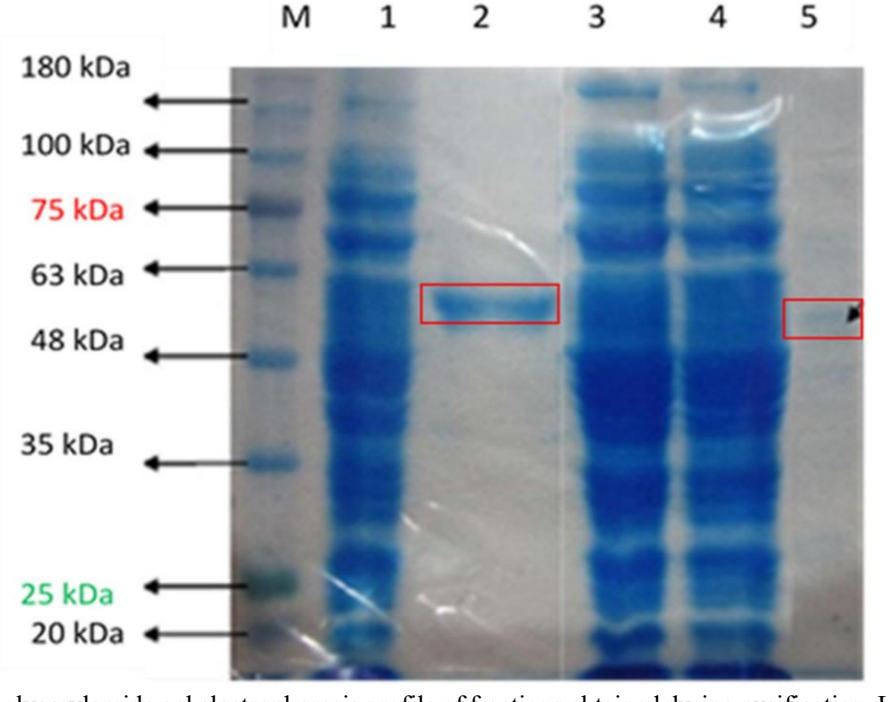

Fig. 7: Sodium dodecyl-polyacrylamide gel electrophoresis profile of fractions obtained during purification. Lane M: protein marker; Lane 1: cell-free GbtXyl43A extract; Lane 2: GbtXyl43A affinity chromatography; Lane 3: cell-free D121N extract; Lane 4: D121N affinity chromatography; Lane 5: D121N anion-exchange chromatography.

Table 8: Purification of GbtXyl43A and D121N.

Protein	Purification step	Total protein (mg)	Total Activity (U)	Specific activity (U/mg)	Yield (%)	Purification (fold)
GbtXyl43A	Cell-free extract	1.914	0.017	0.009	100	1.00
	Affinity chromatography	0.217	0.010	0.046	58.82	5.11
D121N	Cell-free extract	2.914	0.015	0.005	100	1.00
	Affinity chromatography	2.656	0.011	0.004	73.33	0.80
	Anion-exchange chromatography	0.037	4.6×10^{-4}	0.012	3.07	2.40

7), suggesting that D121N had a thinner profile than GbtXyl43A, which was related to the mutation from Asp to Asn at residue 121.

The GbtXyl43A enzyme exhibited an activity of 0.0102 U toward the *p*NP–X substrate, whereas the D121N displayed an activity of 4.6×10^{-4} U. Further data on the comparative activities of the purified enzymes are presented in Table 8. The mutated GbtXyl43A (D121N) exhibited markedly reduced enzyme activity compared to its natural counterpart. The specific activity of D121N was smaller than that of GbtXyl43A, indicating that the Asp mutation substantially affected the catalytic capacity of GbtXyl43A. Additionally, this finding suggests that Asp plays a central role in substrate hydrolysis, and its absence results in the loss of its function as a p*K*a modulator. However, further investigation of the kinetic parameters is necessary to gain further insight into the role of Asp in the catalytic activity against *p*NP–X.

GbtXyl43A achieved a purity level approximately 5 times that of the cell-free extract, with SDS-PAGE analysis showing a single band. In contrast, the D121N mutant exhibited markedly lower purity than GbtXyl43A, requiring an additional purification step with anion exchange to achieve a single-band SDS-PAGE profile. Mutations in Asp destabilized other residues (Table 3), resulting in protein instability (Tables 1 and 2). The reduced stability in less stable proteins increases their tendency to aggregate or denature, leading to a decline in the quality of the purification results. This denaturation can result in the protein interacting nonspecifically with the resin or even forming aggregates. Conversion of Asp-121 to Asn removes its negative charge, changing the surface charge distribution and affecting enzyme affinity for positively charged anion-exchange resins.

An extensive study was performed by mutating Asp-121, which plays an essential role in modulating the p*K*a of general acids and guiding them to the correct orientation to the substrate to identify it.[23] The kinetic parameters of D121N were determined using *p*NP–X as a substrate. The D121N variant was selected for further examination because it exhibited the highest activity among the three mutants.[23] The kinetic reaction of the *p*NP–X substrate by GbtXyl43A and D121N was performed with various substrate concentrations. Increasing substrate concentration increased the rate of product formation. The reaction rate reached its maximum value at relatively high substrate concentrations. Accordingly, a continuous monitoring method was used to ascertain the initial reaction rate, thereby enabling the determination of the kinetic parameters of GbtXyl43A acting on the *p*NP–X substrate.

The kinetic constants for *p*NP–X were determined using Lineweaver–Burk plots (Fig. 8). Table 9 shows the kinetic parameters of GbtXyl43A and D121N, with *p*NP–X as the substrate. GbtXyl43A exhibited kinetic constants for *p*NP–X hydrolysis—2.84 mM and 3.35×10^{-3} mM/min for K_M and V_{max}, respectively. Moreover, D121N exhibited kinetic constants for *p*NP–X hydrolysis—4.56 mM and 0.10×10^{-3} mM/min for K_M and V_{max}, respectively. The K_M value of D121N was higher than that of the wild-type, indicating that its affinity for D121N is lower than that of the wild-type. The elevated K_M value in D121N was due to an amino acid substitution on the catalytic side, resulting in an alteration in enzyme stability, thereby reducing enzyme affinity for the substrate.

The V_{max} value represents the velocity of the product formation of *p*–nitrophenol. The V_{max} value of D121N was lower than that of the wild-type, indicating that the speed of enzymatic reactions involved in *p*–nitrophenol production is slower than that in the wild-type. The k_{cat} values of GbtXyl43A and D121N were 1.97 min^{-1} and 8.40×10^{-4}, respectively. Finally, the catalytic efficiency of the enzyme was determined and expressed as k_{cat}/K_M, which is a measure of substrate specificity. The k_{cat}/K_M values of the wild-type and mutant were 0.69 $min^{-1}mM^{-1}$ and 1.84×10^{-4} $min^{-1}mM^{-1}$, respectively. Lower k_{cat} and k_{cat}/K_M values were expected because of the substitution at the catalytic site.

Asp-121 mutation to Asn had a negative effect on all kinetic parameters. The low V_{max}, k_{cat}, and k_{cat}/K_M values of D121N compared to GbtXyl43A indicated a marked decrease in catalytic activity. The high K_M of D121N indicated that a high substrate concentration was necessary to achieve half of the V_{max} value. The Asp-121 residue plays a central role in substrate–enzyme interactions and the stability of the active site throughout the catalytic reaction. Loss of a negative charge at position 121 likely affects the electrostatic distribution and geometry of the active site, influencing enzymatic hydrolysis of *p*NP–X. No catalytic reaction towards *p*NP–A was observed after the Asp-141 mutation in Xsa43E.[67] A similar phenomenon was observed for XynB3, indicating that the D128G mutant exhibited substantially reduced activity compared to the E187G mutant, an acidic catalytic residue,[55] indicating that Asp-128 plays an essential role in XynB3 and

Table 9: Kinetic parameters summary of *p*–nitrophenyl β–D–xylopyranoside (*p*NP-X) hydrolysis by β-Xylosidase of GbtXyl43A and D121N at 50 °C.

Protein	V_{max} (mM/min)	K_M (mM)	k_{cat} (min^{-1})	k_{cat}/K_M ($min^{-1}mM^{-1}$)
GbtXyl43A	3.35×10^{-3}	2.84	1.97	0.69
D121N	0.10×10^{-3}	4.56	8.40×10^{-4}	1.84×10^{-4}

suggesting that this residue may have an additional role in modulating the p*K*a of Glu-187. Overall, the kinetic data indicated that Asp-121 plays a central role in the catalytic mechanism of GbtXyl43A and as a p*K*a modulator. Asp-128 in XynB3 functions as a p*K*a modulator because of its proximity to the general acid, with 4 Å. Similarly, Asp-121 in GbtXyl43A is located 4.2 Å from the general acid residue, Glu-177. This result corroborates the analogous functions of Asp-128 in XynB3 and Asp-121 in GbtXyl43A as p*K*a modulators of general acid residues.

4. Conclusion

This study revealed that the Asp-121 residue of GbtXyl43A plays a pivotal role in its structural stability and catalytic activity. The mutation of Asp-121 to Glu, Asn, or Val resulted in decreased protein stability and catalytic efficiency, as demonstrated by both in silico and in vitro analyses. Visualization of the surface electrostatic potential illustrated that the Asp-121 mutation altered the charge distribution near the active site, potentially influencing the catalytic mechanism and ligand interactions involving Glu-177 and Asp-14.

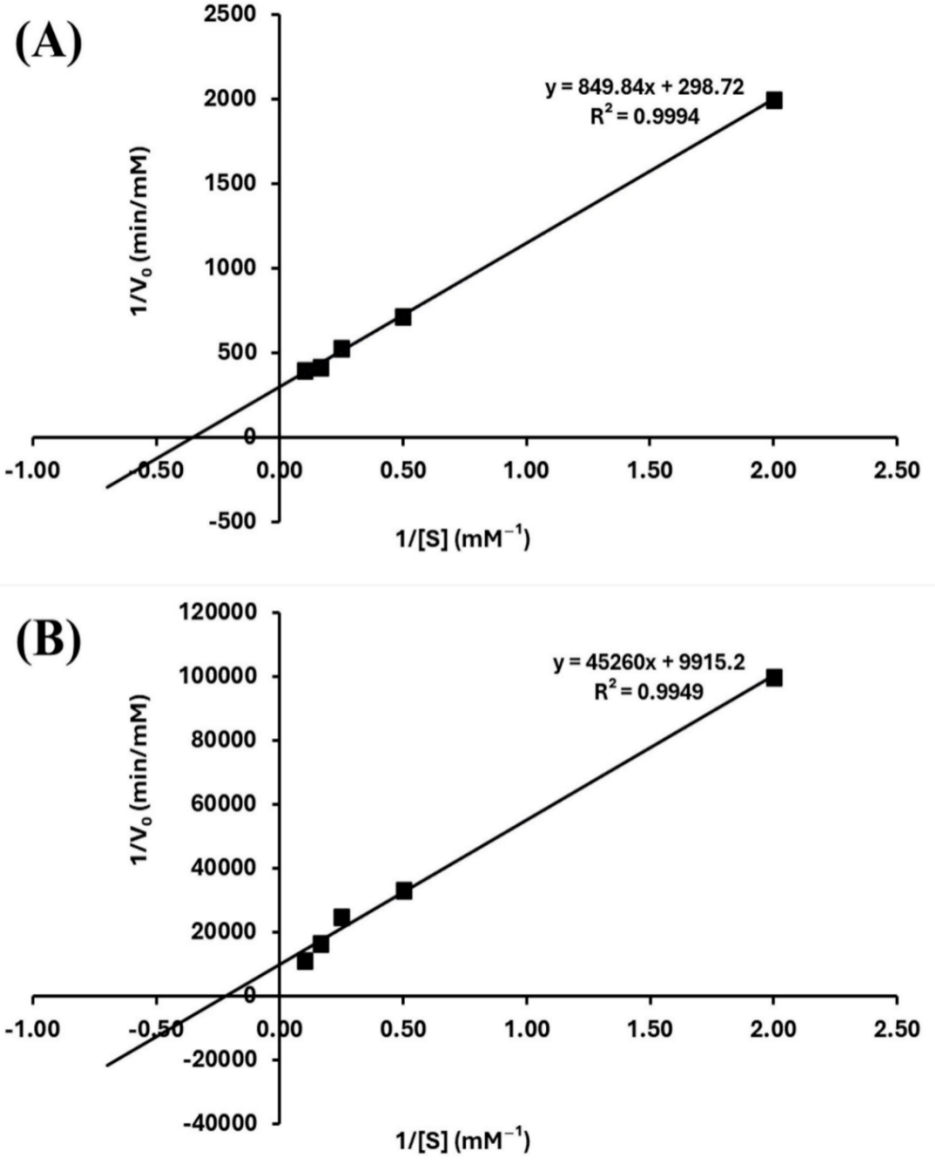

Fig. 8: Lineweaver–Burk plot of kinetic parameter determination of *p*NP–X hydrolysis catalyzed by (A) GbtXyl43A and (B) D121N.

Enzyme kinetics against *p*NP–X confirmed that Asp-121 markedly affects the catalytic activity of GbtXyl43A. The analogous residue Asp-121 in XynB3 (Asp-128) exhibits analogous behavior and acts as a p*K*a modulator. This similarity in implications and roles indicates that Asp-121 plays a role in maintaining structural stability and modulates p*K*a to maintain the electrostatic balance required for efficient catalysis. These findings provide a deeper understanding of the role of Asp-121 as the secondary Asp catalytic residue in the formation of the catalytic triad—Asp-14, Glu-177, and Asp-121—in GbtXyl43A.

Acknowledgments

The authors thank to the Proteomic Laboratory, UCoE-Research Center for Bio-Molecule Engineering, Universitas Airlangga for the research facilities. This study was supported by the International Research Collaboration Top #100 Scheme, Universitas Airlangga (Contract Number: 379/UN3.LPPM/PT. 01.03/2024).

Conflict of Interest

There is no conflict of interest.

Supporting Information

Not applicable.

References

[1] H. Zhang, L. Han, H. Dong, An insight to pretreatment, enzyme adsorption and enzymatic hydrolysis of lignocellulosic biomass: Experimental and modeling studies, *Renewable and Sustainable Energy Reviews*, 2021, **140**, 110758, doi: 10.1016/j.rser.2021.110758.

[2] I. Lawan, W. Zhou, A. L. Idris, Y. Jiang, M. Zhang, L. Wang, Z. Yuan, Synthesis, properties and effects of a multi-functional biodiesel fuel additive, *Fuel Processing Technology*, 2020, **198**, 106228, doi: 10.1016/j.fuproc.2019.106228.

[3] J. Yu, J. Yun, S. Zang, M. Han, X. Sun, Z. Wang, Y. Zhou, A. Khan, M. An, J. Li, S. Chen, Y. Yamauchi, Z. Yuan, Hydrogel fiber fabric combining rapid water transport, thermal localization, and large-scale production for ultra-high salt-resistant solar desalination, *Nano Energy*, 2023, **117**, 108847, doi: 10.1016/j.nanoen.2023.108847.

[4] H. Liao, J. Na, W. Zhou, S. Hur, P. M. Chien, C. Wang, L. Wang, Y. Yamauchi, Z. Yuan, Enhancing energy harvesting performance and sustainability of cellulose-based triboelectric nanogenerators: Strategies for performance enhancement, *Nano Energy*, 2023, **116**, 108769, doi: 10.1016/j.nanoen.2023.108769.

[5] G. Liao, E. Sun, E. B. Gueguim Kana, H. Huang, I. A. Sanusi, P. Qu, H. Jin, J. Liu, L. Shuai, Renewable hemicellulose-based materials for value-added applications, *Carbohydrate Polymers*, 2024, **341**, 122351, doi: 10.1016/j.carbpol.2024.122351.

[6] J. Rao, Z. Lv, G. Chen, F. Peng, Hemicellulose: Structure, chemical modification, and application, *Progress in Polymer Science*, 2023, **140**, 101675, doi: 10.1016/j.progpolymsci.2023.101675.

[7] D. S. Naidu, S. P. Hlangothi, M. J. John, Bio-based products from xylan: a review, *Carbohydrate Polymers*, 2018, **179**, 28-41, doi: 10.1016/j.carbpol.2017.09.064.

[8] S. A. Ellatif, E. S. Abdel Razik, A. A. AL-surhanee, F. Al-Sarraj, G. E. Daigham, A. Y. Mahfouz, Enhanced production, cloning, and expression of a xylanase gene from endophytic fungal strain trichoderma harzianum kj831197.1: unveiling the *in vitro* anti-fungal activity against phytopathogenic fungi, *Journal of Fungi*, 2022, **8**, 447, doi: 10.3390/jof8050447.

[9] T. T. H. Luong, S. Poeaim, N. Tangthirasunun, Isolation and characterization of xylanase from a novel strain, *Penicillium menonorum* SP10, *Mycobiology*, 2023, **51**, 239-245, doi: 10.1080/12298093.2023.2247221.

[10] L. Tsotetsi, R. Prenaven, S. J. Modise, M. Monapathi, Isolation and identification of xylanase producing thermophilic bacteria from compost piles and optimization of xylanase production, *Journal of Biotechnology Research*, 2020, **11**, 57-65.

[11] Y. Zhang, H. Sun, T. Xu, D. Zhao, C. Yu, Y. Zhang, X. Zhang, X. Chen, Y. Zhang, F. Zhao, Gilvimarinus xylanilyticus sp. nov., a novel 1, 3-xylanase-secreting bacterium isolated from a marine green alga, *Frontiers in Microbiology*, 2022, **13**, 1006116, doi: 10.3389/fmicb.2022.1006116.

[12] A. Pasalari, A. Homaei, Isolation and molecular identification of xylanase-producing bacteria from ulva flexuosa of the Persian Gulf, *Processes*, 2022, **10**, 1834, doi: 10.3390/pr10091834.

[13] Y. Huang, X. Zheng, B. Pilgaard, J. Holck, J. Muschiol, S. Li, L. Lange, Identification and characterization of GH11 xylanase and GH43 xylosidase from the chytridiomycetous fungus, Rhizophlyctis rosea, *Applied Microbiology and Biotechnology*, 2019, **103**, 777-791, doi: 10.1007/s00253-018-9431-5.

[14] A. Rohman, B. W. Dijkstra, N. N. T. Puspaningsih, β-xylosidases: structural diversity, catalytic mechanism, and inhibition by monosaccharides, *International Journal of Molecular Sciences*, 2019, **20**, 5524, doi: 10.3390/ijms20225524.

[15] H. Østby, A. Várnai, Hemicellulolytic enzymes in lignocellulose processing, *Essays in Biochemistry*, 2023, **67**, 533-550, doi: 10.1042/ebc20220154.

[16] N. Li, R. Zhang, J. Zhou, Z. Huang, Structures, biochemical characteristics, and functions of β-xylosidases, *Journal of Agricultural and Food Chemistry*, 2023, **71**, 7961-7976, doi: 10.1021/acs.jafc.3c01425.

[17] B. Henrissat, A classification of glycosyl hydrolases based on amino acid sequence similarities, *Biochemical Journal*, 1991, **280**, 309-316, doi: 10.1042/bj2800309.

[18] B. Henrissat, A. Bairoch, New families in the classification of glycosyl hydrolases based on amino acid sequence similarities, *Biochemical Journal*, 1993, **293**, 781-788, doi: 10.1042/bj2930781.

[19] N. N. T. Puspaningsih, H. Suwito, S. Sumarsih, A. Rohman, O. Asmarani, Hidrolisis beberapa jenis xilan dengan enzim xilanolitik termofilik rekombinan, *Berkala Penelitian Hayati*, 2007, **12**, 191-194, doi: 10.23869/bphjbr.12.2.200715.

[20] N. N. T. Puspaningsih, A. Suwanto, M. T. Suhartono, S. S. Achmadi, Yogiara, T. Kimura, Cloning, sequencing, and characterization of the xylan degrading enzymes from *Geobacillus thermoleovorans* IT-08, *Jurnal Ilmu Dasar*, 2008, **9**, 177-185.

[21] A. Rohman, N. van Oosterwijk, N. N. T. Puspaningsih, B. W. Dijkstra, Structural basis of product inhibition by Arabinose and xylose of the thermostable GH43 β-1, 4-xylosidase from Geobacillus thermoleovorans IT-08, *PLoS One*, 2018, **13**, e0196358, doi: 10.1371/journal.pone.0196358.

[22] C. Brüx, A. Ben-David, D. Shallom-Shezifi, M. Leon, K. Niefind, G. Shoham, Y. Shoham, D. Schomburg, The structure of an inverting GH43 β-xylosidase from geobacillus stearothermophilus with its substrate reveals the role of the three catalytic residues, *Journal of Molecular Biology*, 2006, **359**, 97-109, doi: 10.1016/j.jmb.2006.03.005.

[23] L. Hartanti, A. Rohman, A. Suwandi, B. W. Dijkstra, Z. Nurahman, N. N. T. Puspaningsih, Mutation analysis of the pK a modulator residue in β-D-xylosidase from geobacillus thermoleovorans IT-08: activity adaptation to alkaline and high-temperature conditions, *Procedia Chemistry*, 2016, **18**, 39-48, doi: 10.1016/j.proche.2016.01.008.

[24] E. Capriotti, P. Fariselli, R. Casadio, I-Mutant2.0: predicting stability changes upon mutation from the protein sequence or structure, *Nucleic Acids Research*, 2005, **33**, W306-W310, doi: 10.1093/nar/gki375.

[25] J. Cheng, A. Randall, P. Baldi, Prediction of protein stability changes for single-site mutations using support vector machines, *Proteins*: *Structure*, *Function*, *and Bioinformatics*, 2006, **62**, 1125-1132, doi: 10.1002/prot.20810.

[26] G. Li, S. K. Panday, E. Alexov, SAAFEC-SEQ: a sequence-based method for predicting the effect of single point mutations on protein thermodynamic stability, *International Journal of Molecular Sciences*, 2021, **22**, 606, doi: 10.3390/ijms22020606.

[27] C. Chen, M. Lin, C. Liao, H. Chang, Y. Chu, iStable 2.0: Predicting protein thermal stability changes by integrating various characteristic modules, *Computational and Structural Biotechnology Journal*, 2020, **18**, 622-630, doi: 10.1016/j.csbj.2020.02.021.

[28] C. Chen, J. Lin, Y. Chu, iStable: off-the-shelf predictor integration for predicting protein stability changes, *BMC Bioinformatics*, 2013, **14**, S5, doi: 10.1186/1471-2105-14-S2-S5.

[29] D. E. V. Pires, D. B. Ascher, T. L. Blundell, DUET: a server for predicting effects of mutations on protein stability using an integrated computational approach, *Nucleic Acids Research*, 2014, **42**, W314-W319, doi: 10.1093/nar/gku411.

[30] V. Parthiban, M. M. Gromiha, D. Schomburg, CUPSAT: prediction of protein stability upon point mutations, *Nucleic Acids Research*, 2006, **34**, W239-W242, doi: 10.1093/nar/gkl190.

[31] M. Philipp, C. W. Moth, N. Ristic, J. K. S. Tiemann, F. Seufert, A. Panfilova, J. Meiler, P. W. Hildebrand, A. Stein, D. Wiegreffe, R. Staritzbichler, MutationExplorer: a webserver for mutation of proteins and 3D visualization of energetic impacts, *Nucleic Acids Research*, 2024, **52**, W132-W139, doi: 10.1093/nar/gkae301.

[32] S. Bienert, A. Waterhouse, T. A. P. de Beer, G. Tauriello, G. Studer, L. Bordoli, T. Schwede, The SWISS-MODEL repository: new features and functionality, *Nucleic Acids Research*, 2017, **45**, D313-D319, doi: 10.1093/nar/gkw1132.

[33] A. Waterhouse, M. Bertoni, S. Bienert, G. Studer, G. Tauriello, R. Gumienny, F. T. Heer, T. A. P. de Beer, C. Rempfer, L. Bordoli, R. Lepore, T. Schwede, SWISS-MODEL: homology modelling of protein structures and complexes, *Nucleic Acids Research*, 2018, **46**, W296-W303, doi: 10.1093/nar/gky427.

[34] L. Bordoli, T. Schwede, Automated protein structure modeling with SWISS-MODEL workspace and the protein model portal, *Homology Modeling. Methods in Molecular Biology*, Humana Press, New Jersey, 2011, 107-136, ISBN: 978-1-61779-588-6.

[35] M. Biasini, S. Bienert, A. Waterhouse, K. Arnold, G. Studer, T. Schmidt, F. Kiefer, T. G. Cassarino, M. Bertoni, L. Bordoli, T. Schwede, SWISS-MODEL: modelling protein tertiary and quaternary structure using evolutionary information, *Nucleic Acids Research*, 2014, **42**, W252-W258, doi: 10.1093/nar/gku340.

[36] N. Guex, M. C. Peitsch, T. Schwede, Automated comparative protein structure modeling with SWISS-MODEL and Swiss-PdbViewer: A historical perspective, *Electrophoresis*, 2009, **30**, S162-S173, doi: 10.1002/elps.200900140

[37] M. U. Johansson, V. Zoete, O. Michielin, N. Guex, Defining and searching for structural motifs using DeepView/Swiss-PdbViewer, *BMC Bioinformatics*, 2012, **13**, 173, doi: 10.1186/1471-2105-13-173.

[38] N. F. S. K. Anuar, R. A. Wahab, F. Huyop, K. B. A. Halim, A. A. A. Hamid, *In silico* mutation on a mutant lipase from *Acinetobacter haemolyticus* towards enhancing alkaline stability, *Journal of Biomolecular Structure and Dynamics*, 2020, **38**, 4493-4507, doi: 10.1080/07391102.2019.1683074.

[39] K. Batumalaie, M. F. Edbeib, N. A. Mahat, F. Huyop, R. A. Wahab, *In silico*and empirical approaches toward understanding the structural adaptation of the alkaline-stable lipase KV1 from *Acinetobacter haemolyticus*, *Journal of Biomolecular Structure and Dynamics*, 2018, **36**, 3077-3093, doi: 10.1080/07391102.2017.1377635.

[40] R. A. Laskowski, M. W. MacArthur, D. S. Moss, J. M. Thornton, PROCHECK: a program to check the stereochemical quality of protein structures, *Journal of Applied Crystallography*,1993, **26**, 283-291, doi: 10.1107/s0021889892009944.

[41] B. Dutta, A. Banerjee, P. Chakraborty, R. Bandopadhyay, *In silico* studies on bacterial xylanase enzyme: Structural and functional insight, *Journal of Genetic Engineering and Biotechnology*, 2018, **16**, 749-756, doi: 10.1016/j.jgeb.2018.05.003.

[42] M. Wiederstein, M. J. Sippl, ProSA-web: interactive web service for the recognition of errors in three-dimensional structures of proteins, *Nucleic Acids Research*, 2007, **35**, W407-W410, doi: 10.1093/nar/gkm290.

[43] K. Pramanik, P. K. Ghosh, S. Ray, A. Sarkar, S. Mitra, T. K. Maiti, An in silico structural, functional and phylogenetic analysis with three dimensional protein modeling of alkaline phosphatase enzyme of Pseudomonas aeruginosa, *Journal of Genetic Engineering and Biotechnology*, 2017, **15**, 527-537, doi: 10.1016/j.jgeb.2017.05.003.

[44] J. Eberhardt, D. Santos-Martins, A. F. Tillack, S. Forli, AutoDock vina 1.2.0: new docking methods, expanded force field, and Python bindings, *Journal of Chemical Information and Modeling*, 2021, **61**, 3891-3898, doi: 10.1021/acs.jcim.1c00203.

[45] O. Trott, A. J. Olson, AutoDock Vina: Improving the speed and accuracy of docking with a new scoring function, efficient optimization, and multithreading, *Journal of Computational Chemistry*, 2010, **31**, 455-461, doi: 10.1002/jcc.21334.

[46] R. A. Laskowski, M. B. Swindells, LigPlot+: multiple ligand–protein interaction diagrams for drug discovery, *Journal of Chemical Information and Modeling*, 2011, **51**, 2778-2786, doi: 10.1021/ci200227u.

[47] J. M. Manns, SDS-polyacrylamide gel electrophoresis (SDS-PAGE) of proteins, *Current Protocols in Microbiology*, 2011, **22**, 1-13, doi: 10.1002/9780471729259.mca03ms22.

[48] N. Kresge, R. D. Simoni, R. L. Hill, SDS-PAGE to determine the molecular weight of proteins: the work of klaus weber and Mary Osborn, *Journal of Biological Chemistry*, 2006, **281**, e19-e21, doi: 10.1016/S0021-9258(20)55866-3.

[49] C. L. Kielkopf, W. Bauer, I. L. Urbatsch, Bradford assay for determining protein concentration, *Cold Spring Harbor Protocols*, 2020, **2020**, pdb.prot102269, doi: 10.1101/pdb.prot102269.

[50] O. Ernst, T. Zor, Linearization of the Bradford protein assay, *Journal of Visualized Experiments*, 2010, **38**, e1918, doi: 10.3791/1918.

[51] T. Zor, Z. Selinger, Linearization of the Bradford protein assay increases its sensitivity: theoretical and experimental studies, *Analytical Biochemistry*, 1996, **236**, 302-308, doi: 10.1006/abio.1996.0171.

[52] M. M. Bradford, A rapid and sensitive method for the quantitation of microgram quantities of protein utilizing the principle of protein-dye binding, *Analytical Biochemistry*, 1976, **72**, 248-254, doi: 10.1016/0003-2697(76)90527-3.

[53] A. Rohman, N. van Oosterwijk, S. Kralj, L. Dijkhuizen, B. W. Dijkstra, N. N. T. Puspaningsih, Purification, crystallization and preliminary X-ray analysis of a thermostable glycoside hydrolase family 43 β-xylosidase from*Geobacillus thermoleovorans*IT-08, *Acta Crystallographica Section F Structural Biology and Crystallization Communications*, 2007, **63**, 932-935, doi: 10.1107/s1744309107046015.

[54] D. Nurizzo, J. P. Turkenburg, S. J. Charnock, S. M. Roberts, E. J. Dodson, V. A. McKie, E. J. Taylor, H. J. Gilbert, G. J. Davies, Cellvibrio japonicus α-L-arabinanase 43A has a novel five-blade β-propeller fold, *Nature Structural Biology*, **9**, 665-668, doi: 10.1038/nsb835.

[55] D. Shallom, M. Leon, T. Bravman, A. Ben-David, G. Zaide, V. Belakhov, G. Shoham, D. Schomburg, T. Baasov, Y. Shoham, Biochemical characterization and identification of the catalytic residues of a family 43 β-d-xylosidase from *Geobacillus stearothermophilus* T-6, *Biochemistry*, 2005, **44**, 387-397, doi: 10.1021/bi048059w.

[56] M. R. Proctor, E. J. Taylor, D. Nurizzo, J. P. Turkenburg, R. M. Lloyd, M. Vardakou, G. J. Davies, H. J. Gilbert, Tailored catalysts for plant cell-wall degradation: Redesigning the exo/endo preference of*Cellvibrio japonicus*arabinanase 43A, *Proceedings of the National Academy of Sciences of the United States of America*, 2005, **102**, 2697-2702, doi: 10.1073/pnas.0500051102.

[57] P. Benkert, M. Biasini, T. Schwede, Toward the estimation of the absolute quality of individual protein structure models, *Bioinformatics*, 2011, **27**, 343-350, doi: 10.1093/bioinformatics/btq662.

[58] G. Davies, B. Henrissat, Structures and mechanisms of glycosyl hydrolases, *Structure*, 1995, **3**, 853-859, doi: 10.1016/S0969-2126(01)00220-9.

[59] M. A. B. Morais, J. Coines, M. N. Domingues, R. A. S. Pirolla, C. C. C. Tonoli, C. R. Santos, J. B. L. Correa, F. C. Gozzo, C. Rovira, M. T. Murakami, Two distinct catalytic pathways for GH43 xylanolytic enzymes unveiled by X-ray and QM/MM simulations, *Nature*, 2021, **12**, 367, doi: 10.1038/s41467-020-20620-3.

[60] P. Falck, J. A. Linares-Pastén, P. Adlercreutz, E. N. Karlsson, Characterization of a family 43 β-xylosidase from the xylooligosaccharide utilizing putative probiotic *Weissella* sp. strain 92, *Glycobiology*, 2016, **26**, 193-202, doi: 10.1093/glycob/cwv092.

[61] A. A. I. Ratnadewi, M. Fanani, S. D. Kurniasih, M. Sakka, E. B. Wasito, K. Sakka, Z. Nurachman, N. N. T. Puspaningsih, β-d-xylosidase from *Geobacillus thermoleovorans* IT-08: biochemical characterization and bioinformatics of the enzyme, *Applied Biochemistry and Biotechnology*, 2013, **170**, 1950-1964, doi: 10.1007/s12010-013-0329-5.

[62] S. S. Chaturvedi, D. Bím, C. Z. Christov, A. N. Alexandrova, From random to rational: improving enzyme design through electric fields, second coordination sphere interactions, and conformational dynamics, *Chemical Science*, 2023, **14**, 10997-11011, doi: 10.1039/d3sc02982d.

[63] T. A. Coulther, J. Ko, M. J. Ondrechen, Amino acid interactions that facilitate enzyme catalysis, *The Journal of Chemical Physics*, 2021, **154**, 195101, doi: 10.1063/5.0041156.

[64] W. Lin, Q. Wang, R. Han, J. Zhou, G. Xu, Y. Ni, Engineering of methionine adenosyltransferase reveals key roles of electrostatic interactions in enhanced catalytic activity, *Applied Biochemistry and Biotechnology*, 2024, **196**, 3246-3259, doi: 10.1007/s12010-023-04676-7.

[65] D. Suplatov, N. Panin, E. Kirilin, T. Shcherbakova, P. Kudryavtsev, V. Švedas, Computational design of a pH stable enzyme: understanding molecular mechanism of penicillin acylase's adaptation to alkaline conditions, *PLoS One*, 2014, **9**, e100643, doi: 10.1371/journal.pone.0100643.

[66] X. Chen, J. Liao, Y. Lin, J. Zhang, C. Zheng, Nanozyme's catalytic activity at neutral pH: reaction substrates and application in sensing, *Analytical and Bioanalytical Chemistry*, 2023, **415**, 3817-3830, doi: 10.1007/s00216-023-04525-w.

[67] M. Till, D. Goldstone, G. Card, G. T. Attwood, C. D. Moon, V. L. Arcus, Structural analysis of the GH43 enzyme Xsa43E from *Butyrivibrio proteoclasticus*, *Acta Crystallographica Section F Structural Biology Communications*, 2014, **70**, 1193-1198, doi: 10.1107/s2053230x14014745.